nature climate change

FOCUS | ARTICLES

https://doi.org/10.1038/s41558-021-01026-5

Check for updates

Carbon loss from forest degradation exceeds that from deforestation in the Brazilian Amazon

Yuanwei Qin[1], Xiangming Xiao[1✉], Jean-Pierre Wigneron[2✉], Philippe Ciais[3], Martin Brandt[4], Lei Fan[5], Xiaojun Li[2], Sean Crowell[6], Xiaocui Wu[1], Russell Doughty[1,7], Yao Zhang[8], Fang Liu[9], Stephen Sitch[10] and Berrien Moore III[6]

Spatial–temporal dynamics of aboveground biomass (AGB) and forest area affect the carbon cycle, climate and biodiversity in the Brazilian Amazon. Here we investigate interannual changes in AGB and forest area by analysing satellite-based annual AGB and forest area datasets. We found that the gross forest area loss was larger in 2019 than in 2015, possibly due to recent loosening of forest protection policies. However, the net AGB loss was three times smaller in 2019 than in 2015. During 2010–2019, the Brazilian Amazon had a cumulative gross loss of 4.45 Pg C against a gross gain of 3.78 Pg C, resulting in a net AGB loss of 0.67 Pg C. Forest degradation (73%) contributed three times more to the gross AGB loss than deforestation (27%), given that the areal extent of degradation exceeds that of deforestation. This indicates that forest degradation has become the largest process driving carbon loss and should become a higher policy priority.

Tropical forests in the Amazon account for approximately 50% of the rainforests in the world[1] and are important for global biodiversity, hydrology, climate and the carbon cycle[2–6]. Accurate and timely data on vegetation aboveground biomass (AGB) and forest area in the region at various spatial and temporal scales are needed to understand the carbon balance, which is affected by land use, logging and degradation, secondary forest regrowth, and climate[7,8]. In addition to in situ AGB measurements in intact forests[9–11], several studies combined in situ AGB data with images from optical, microwave and laser sensors to generate static AGB maps over merged periods (for example, circa 2000 (ref. [3]), circa 2007–2008 (ref. [12]) and 2003–2014 (ref. [13])). Combined with forest area change datasets from the Amazon Deforestation Monitoring Project (PRODES)[14] and the Global Forest Watch (GFW)[15], these static AGB maps are used to estimate AGB dynamics from deforestation and forest degradation[13,16], but forest losses from PRODES were substantially smaller than those from GFW[17–19]. These differences and uncertainties result from different forest definitions and the use of Landsat images, which are severely impacted by frequent clouds and aerosols from fire, leaving very few good-quality images per year[17]. This issue could be solved by the use of Moderate Resolution Imaging Spectroradiometer (MODIS) data. The spatial resolution of these data cannot identify small patches of forest losses or gains, but the daily images ensure more good-quality observations per year[17].

Substantial progress has been made in analysing L-band vegetation optical depth (L-VOD) from the Soil Moisture and Ocean Salinity (SMOS) passive microwave images, which provide annual maps of AGB since 2010 at 0.25° spatial resolution (Methods)[20–23]. Moreover, images from the Phased Array type L-band Synthetic Aperture Radar (PALSAR) and MODIS were used to derive annual maps of evergreen forest areas at 500-m resolution for the Brazilian Amazon during 2000–2017 (refs. [17,24]). Combining L-VOD AGB and PALSAR/MODIS forest area during 2010–2019 offers a unique window to assess the spatial–temporal dynamics of AGB and forest area in the Brazilian Amazon and how these dynamics are impacted by climate and land use. This period is of special interest, because the impacts on forest area and biomass from extreme climate events and the changed policies of the new Brazilian government (in office since January 2019), favouring the expansion of pasture[25,26] at the expense of forest conservation, have not yet been fully quantified.

Here we used the annual L-VOD AGB[20] and annual forest area datasets[17] described above to investigate the spatial–temporal dynamics of forest carbon in the Brazilian Amazon during 2010–2019. We investigated (1) the role of climate anomalies in the changes in forest area and AGB (for example, the Atlantic Multi-decadal Oscillation (2010), El Niño (2009–2010 and 2015–2016) and La Niña (2010–2011 and 2017)) (Extended Data Fig. 1); (2) whether recent changes in policies and human activities in 2019 have a detectable effect on forest area and AGB; and (3) the relative contributions of deforestation and forest degradation (forest fragmentation, edge effects, logging, forest fire and drought) to interannual variation in AGB loss in the study period.

Consistency between AGB and forest area

The AGB and forest area data were organized into 5,656 grid cells at 0.25° spatial resolution (~25 km × 25 km) (Methods). We studied the relationships between annual AGB and forest area fraction (FAF) for individual grid cells. The spatial distribution of AGB agrees well with that of FAF in 2019 (Fig. 1a,b). AGB and FAF are linearly (spatially) correlated with each other in 2019 and other years (Fig. 1c and Extended Data Fig. 2, $R^2 \geq 0.81$). We also investigated the temporal consistency between AGB and FAF for all grid cells over the ten years. As an example, we showed two contrasting grid cells that exhibited either a large loss (Fig. 2a–c) or a large gain (Fig. 2d–f) in FAF. The temporal correlation between AGB

[1]Department of Microbiology and Plant Biology, Center for Earth Observation and Modeling, University of Oklahoma, Norman, OK, USA. [2]ISPA, UMR 1391, INRA Nouvelle-Aquitaine, Bordeaux Villenave d'Ornon, France. [3]Laboratoire des Sciences du Climat et de l'Environnement, LSCE/IPSL, CEA-CNRS-UVSQ, Université Paris-Saclay, Gif-sur-Yvette, France. [4]Department of Geosciences and Natural Resource Management, University of Copenhagen, Copenhagen, Denmark. [5]Chongqing Jinfo Mountain Karst Ecosystem National Observation and Research Station, School of Geographical Sciences, Southwest University, Chongqing, China. [6]College of Atmospheric and Geographic Sciences, University of Oklahoma, Norman, OK, USA. [7]Division of Geological and Planetary Sciences, California Institute of Technology, Pasadena, CA, USA. [8]Climate and Ecosystem Sciences Division, Lawrence Berkeley National Laboratory, Berkeley, CA, USA. [9]Institute of Geographic Sciences and Natural Resources Research, Chinese Academy of Sciences, Beijing, China. [10]College of Life and Environmental Sciences, University of Exeter, Exeter, UK. ✉e-mail: xiangming.xiao@ou.edu; jean-pierre.wigneron@inrae.fr

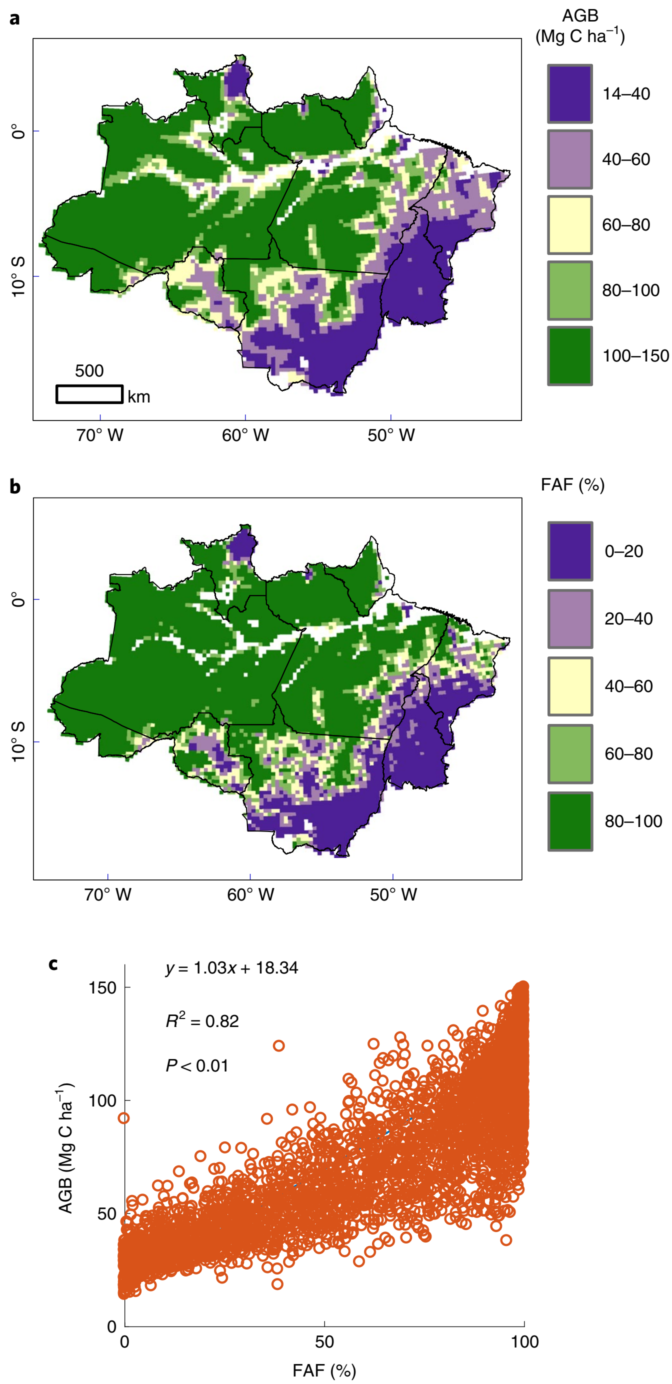

Fig. 1 | Spatial distributions of AGB and FAF and their linear regression relationship within 0.25° (~25 km × 25 km) grid cells. a, Spatial distribution of averaged AGB (Mg C ha^{-1}) in 2019. **b**, Spatial distribution of FAF (%) in 2019. **c**, Linear regression analysis between AGB and FAF in 2019 (number of pixels: 5,656).

and FAF (AGB = f(FAF)) was found to be strong in the 'loss' grid cell ($R^2 = 0.82$, $P < 0.01$) and lower but significant in the 'gain' grid cell ($R^2 = 0.30$, $P < 0.1$). The spatial distributions of the temporal relationships between AGB and FAF during 2010–2019 are shown in Fig. 2g,h. We found that 23% of the total area (112×10^6 ha) had a statistically significant ($P < 0.05$) and positive linear relationship between AGB and FAF, especially in the southern and eastern Brazilian Amazon. This loss of AGB following forest area losses is expected, but the slope of the relationship differs depending on the mechanisms that lead to forest area loss and exposed AGB densities. Conversely, intact forest with no forest area loss can have changes in AGB due to climate anomalies or forest degradation. At 25-km spatial resolution, we observed only the bulk of AGB changes, and further work is needed to attribute the roles of forest area loss, forest area gain and forest degradation on top of climate-induced variability. In the following sections, we take a closer look at yearly anomalies to gain insights on those drivers.

Interannual changes in AGB and forest area

The interannual changes in forest area, active fire area, burned area and AGB are displayed in Fig. 3. We decomposed the annual net AGB change into the sum of gross AGB loss (grid cells with negative changes) and gross gain (grid cells with positive changes). The gross forest area loss in 2019 (3.9×10^6 ha), which was a drought year, was larger than that during the extreme El Niño drought year of 2015 (3.0×10^6 ha) (Fig. 3c). This suggests that the combined impacts of policy changes by the Brazilian government[25,26] and drought (that is, drought-induced tree mortality and enhanced forest fires) caused a larger forest area loss in 2019. In contrast, the net AGB change in 2019 (−0.05 Pg C) was only one-fifth of the net AGB change in 2015 (−0.25 Pg C) (Fig. 3d), which is confirmed by the large gross AGB loss (−0.55 Pg C) in 2015 (Fig. 3d and Extended Data Fig. 3). The strong El Niño in 2015 thus resulted in a more extensive loss of AGB over both intact and secondary forests, from drought and drought-induced fires coordinated with human ignitions[27]. Comparing losses of AGB and forest area changes in 2014–2015 and 2018–2019 revealed that the extreme El Niño in 2015 and the combined impact of policy changes and drought in 2019 had differential impacts on AGB and forest area. As 2019 was the first year of Brazilian president Jair Bolsonaro's administration, the impacts of those policy changes on AGB and forest area remain to be investigated beyond 2020.

Over the ten-year period, linear regression analysis showed a strong correlation between annual AGB and forest area (Fig. 3a, $R^2 = 0.78$). Annual AGB decreased from 44.86 Pg C in 2010 to 44.19 Pg C in 2019, a net loss of 0.67 Pg C (0.07 Pg C yr^{-1}), while annual forest area decreased from 370.21×10^6 ha in 2010 to 361.29×10^6 ha in 2019, a net loss of 8.91×10^6 ha (0.99×10^6 ha yr^{-1}) (Fig. 3a). These total numbers mask the highly dynamic and regional nature of interannual changes in gross gains and gross losses of AGB and forest area, which partly compensate for each other. We thus calculated interannual changes in AGB (Fig. 3d) and forest area (Fig. 3c) between two consecutive years for individual grid cells and identified gross gains and gross losses as the sums of AGB changes in all the grid cells showing either gains or losses (Fig. 3e). On average, gross AGB loss and gain (Fig. 3e) were about five times larger than net changes between two years (Fig. 3d). The cumulated gross loss and gross gain of AGB in the Brazilian Amazon over 2010–2019 were 4.45 Pg C and 3.78 Pg C, respectively.

The cumulated gross forest area loss over the ten years was about 19.75×10^6 ha (Fig. 3e). The GFW[18] reported loss (19.14×10^6 ha during 2010–2018) is very close to our estimate. PRODES reported only 6.72×10^6 ha in forest area loss during 2010–2019 (ref. [14]); this is because it was designed to monitor only deforestation of old-growth primary forests as per 1988, not considering losses from secondary forests, which have a high turnover and can get deforested several times within our study period[28]. The GFW and our MODIS forest area datasets include losses of primary and secondary forests since 2000 and 2001, respectively. From 1988 to 2000, some pixels classified as intact forest in 1988 by PRODES may have already been deforested and regenerated when their dynamics are monitored by MODIS and GFW products.

We calculated the temporal dynamics of AGB and FAF for six classes of FAF (Methods) and found that AGB varied temporally in tandem with FAF (Extended Data Fig. 4), suggesting that interannual changes in forest area are one of the major factors contributing

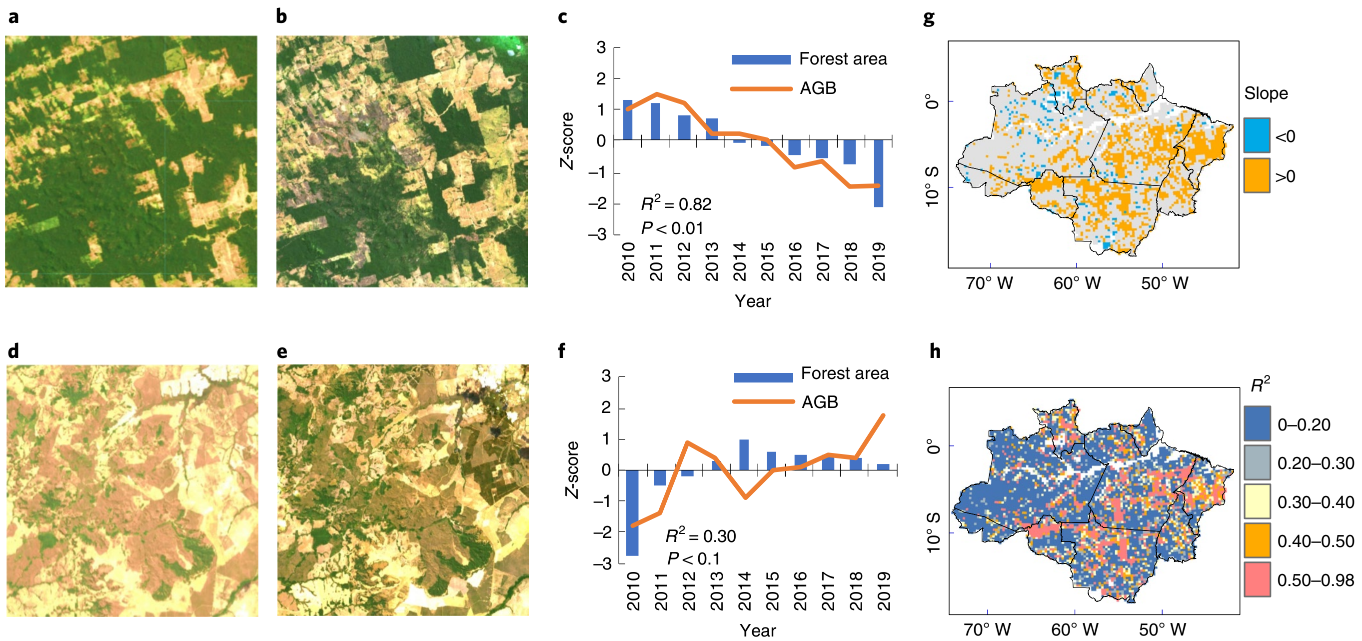

Fig. 2 | Interannual variation of FAF and AGB during 2010–2019. a–f, Two ~25-km × 25-km grid cells with forest area loss (**a** and **b**; central latitude, 6.7° S; longitude, 55.2° W) and forest gain (**d** and **e**; central latitude, 17.4° S; longitude, 53.4° W). In **a** and **b**, USGS/NASA Landsat images acquired on 3 July 2010 and 9 August 2019 (ref. [52]) are shown, and **c** shows the annual anomaly values (*Z*-score) of forest area and AGB in the forest area loss grid cell (**a** and **b**). In **d** and **e**, Landsat images acquired on 27 August 2010 and 5 September 2019 (ref. [52]) are shown, and **f** shows the annual anomaly values (*Z*-score) of forest area and AGB in the forest area gain grid cell (**d** and **e**). **g**, Map of the linear regression slope between annual FAF and AGB during 2010–2019. The grey grid cells have temporal R^2 less than 0.3. **h**, Map of temporal R^2 between annual FAF and AGB during 2010–2019.

to interannual changes in AGB. The interannual variations of active fire and burned areas (Fig. 3b) corresponded well with those of annual AGB and forest area losses during 2010–2019, except in 2017 and 2019 (Fig. 3c,d), indicating that fire was strongly associated with the losses of AGB and forest area.

AGB and forest area losses in El Niño years

The impacts of El Niño climate events on vegetation have been debated intensively over the past few decades[10,11,27,29,30]. Seasonally moist Amazonian forests have deep root systems that could use water in deep soils, and they have a relatively high resilience to drought[11,31]. We calculated interannual changes in AGB and forest area between the 2015 extreme El Niño year and the previous year (Extended Data Fig. 1a). The net AGB change was negative and larger in 2015 (−0.25 Pg C), with a gross AGB loss of 0.55 Pg C that surpassed a modest gross AGB gain of 0.29 Pg C (Fig. 3d). The net forest area change (-5.79×10^6 ha) was also large in 2015. We detected a much larger loss of forest area in 2015 than in 2016, but the GFW and PRODES datasets showed smaller losses of forest area in 2015 than in 2016 (Extended Data Fig. 5). This discrepancy can be attributed to different definitions of forest[16], mapping algorithms (PRODES excludes secondary forest loss), calendar year (PRODES uses August of the current year to July of the subsequent year) and the limited number of Landsat images used by the GFW and PRODES projects. The larger loss of AGB (Fig. 3a), larger active fire area and burned area (Fig. 3b), and larger annual growth rate of atmospheric CO_2 concentration (Fig. 3f and Extended Data Fig. 6) in 2015 support our finding of a larger loss of forest area in 2015 than in 2016.

To identify hotspots of AGB and forest area change in 2015, we calculated the changes in average AGB and forest area during 2010–2013 and during 2015–2018 (Fig. 4a,b). The spatial distribution of AGB change (Fig. 4a) matched well with that of forest area change in the 'Arc of Deforestation' (Fig. 4b). Between these two periods, AGB gain occurred in 29.40% of the area (141.71×10^6 ha) and AGB loss in 70.60% (340.26×10^6 ha) (Fig. 4a). Forest area gain occurred in 15.43% of the area (74.39×10^6 ha) and forest area loss in 51.63% (248.82×10^6 ha) (Fig. 4b). In this time, 44.78% of the Brazilian Amazon had both AGB and forest area loss (Fig. 4c). The relationship between AGB and forest area changes between these two periods was statistically significant ($P < 0.01$) but weakly correlated (Fig. 4c). This partial decoupling between AGB and forest area happens because few grid cells have large losses of AGB and forest area, while many others have a small loss of forest area and a moderate loss of AGB (Fig. 4d). These results show that in 2015, the contribution of deforestation to the AGB loss was moderate ($R^2 = 0.19$), suggesting that climate-induced tree mortality and degradation contributed to the AGB loss.

We further analysed the interannual changes in AGB in those grid cells with stable forest area in relation to changes in mean annual precipitation and mean maximum cumulative water deficit (MCWD) (Methods) in 2010–2013 and 2015–2018 (Fig. 4e, Supplementary Figs. 1 and 2, and Extended Data Fig. 7). Approximately 37% of this area (58.37×10^6 ha) had AGB gains (0.06 Pg C; 0.49 Mg C ha^{-1} yr^{-1}), most of which were distributed in the northwest (Fig. 4a,b), where the mean annual precipitation was higher than 2,000 mm yr^{-1} (Supplementary Fig. 1). The remaining areas with no forest area change (63%; 99.53×10^6 ha) had AGB losses (0.14 Pg C; 0.70 Mg C ha^{-1} yr^{-1}), suggesting that extensive forest degradation occurred. AGB loss increased as annual precipitation decreased, indicating that drought was a driver of forest degradation, and grid cells with an annual precipitation of <2,000 mm yr^{-1} had the largest sensitivity to drought (Fig. 4e). Approximately 85% of fires consistently occurred in the region with an annual precipitation of <2,000 mm yr^{-1}, and there was a 70% increase of fires in the region with an annual precipitation of ≥2,000 mm yr^{-1}, which can also explain AGB loss patterns in El Niño years[27]. In addition, for grid cells with forest area losses between the pre- and post-2015 El Niño periods, AGB losses between these periods were impacted

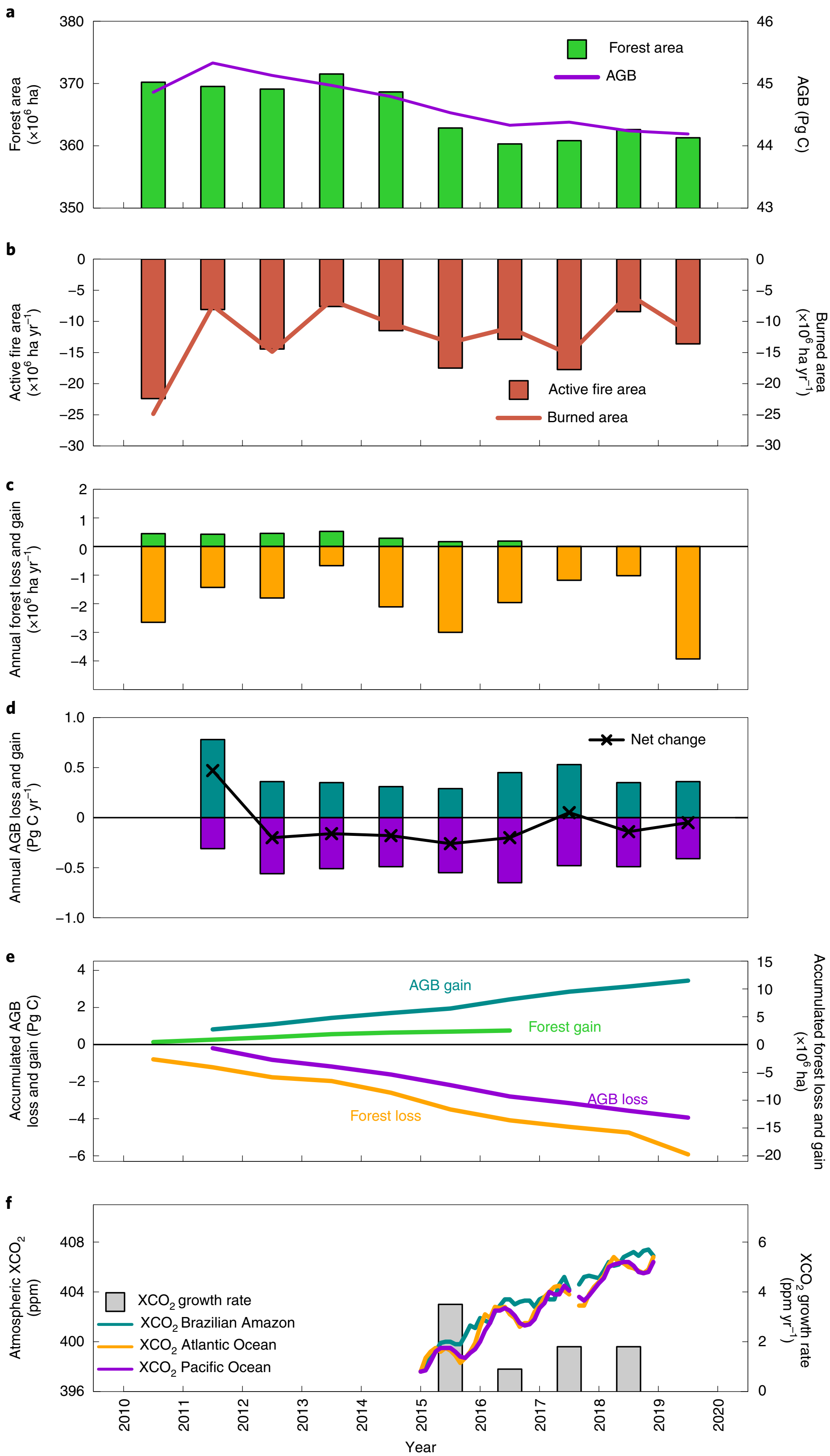

Fig. 3 | Interannual variations of annual AGB and forest area in the Brazilian Amazon during 2010–2019. a, Annual AGB estimated from L-VOD data and forest area estimated from MODIS data for each year. **b**, Annual active fire area estimated by MOD14A2 and annual burned area estimated by MCD64A1. **c**, Annual gross forest area loss and gain. **d**, Interannual AGB changes (gross gain, gross loss and net change). **e**, Accumulated gross loss and gain of AGB and forest area. **f**, Monthly atmospheric XCO_2 from OCO-2 observations in the Brazilian Amazon, Atlantic Ocean and Pacific Ocean. To make the figure clear, we did not show the standard deviation values.

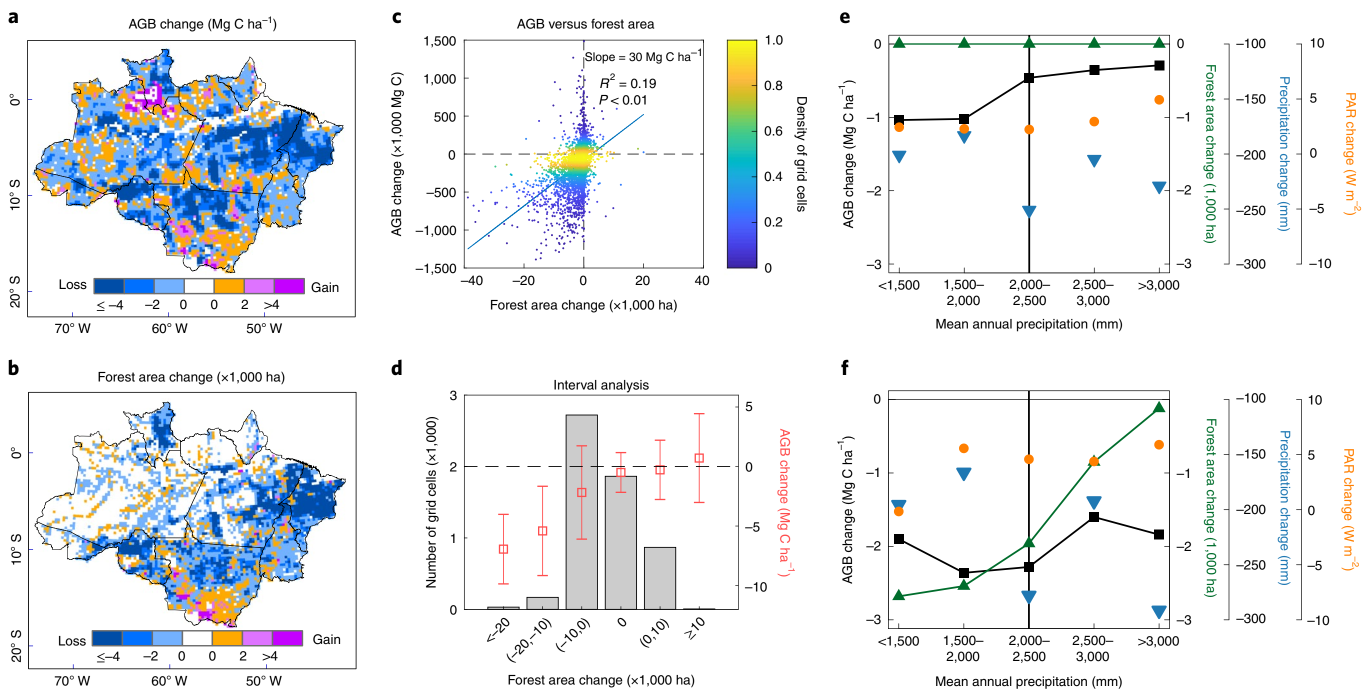

Fig. 4 | The changes in average AGB and forest area within 0.25° (~25 km × 25 km) grid cells before and after the 2015 extreme El Niño in 2010–2013 and 2015–2018. **a**, Spatial distribution of the AGB change as the difference between the second and first periods. **b**, Spatial distribution of forest area change. **c**, Scatter plot and regression between forest area and AGB changes across grid cells. **d**, Grid cell numbers (grey bars) for different bins of forest area change and average values and standard deviations of AGB change. **e**, AGB, forest area, precipitation and photosynthetically active radiation (PAR) changes only for grid cells with no forest area change grouped into different bins of mean annual precipitation (500-mm intervals). **f**, Same as **e** but for grid cells with a forest area loss of up to 10×10^3 ha between the two periods.

by climate, deforestation and human-induced forest degradation, which tended to be higher in areas with precipitation in the range of 1,500–2,500 mm yr^{-1} (Fig. 4f). Similar results are obtained with MCWD instead of mean annual rainfall (Extended Data Fig. 7). Further analyses of new land cover and degradation datasets[28,32] are needed to attribute these bulk reductions of AGB to the different drivers and their interactions affecting forests in different regions of the Brazilian Amazon.

The 2015–2016 El Niño caused widespread AGB losses in 63% of the Brazilian Amazon. We calculated the recovery strength[22] in the following three years and found that AGB fully recovered only in 25% of the area (Extended Data Fig. 8). The moist forest in the northwest and the Cerrado area in the southeast recovered quickly. In contrast, the 'Arc of Deforestation' region, where fires also peaked during the El Niño, did not show a recovery of AGB. In this region, deforested areas from intact or secondary forests are primarily used for crops and pasture. Recent data show that secondary forests did regrow but were frequently deforested again[28].

Increased AGB in La Niña years

Several local studies investigated the speed of vegetation recovery in the Amazon after El Niños[10,11,33]. Our data with full coverage of the region show that forest area changed little between 2010 and 2012, but annual AGB in the strong La Niña of 2011 was higher (by 0.47 Pg C) than in the drought year of 2010 (Fig. 3a,d). Field data from long-term forest plots reported slightly higher forest growth in 2011 than in 2010 (ref. [10]). Results from atmospheric inversion suggested that in 2011 the Amazon basin was a net CO_2 sink of 0.25 ± 0.14 Pg C yr^{-1}, higher than in 2010 (ref. [34]). Similarly, annual AGB during the 2017 La Niña was also slightly higher (by 0.05 Pg C) than in the previous year, but this signal is mixed with the legacy effects of the 2015 El Niño (Fig. 3a). We also analysed atmospheric CO_2 concentration data over the Amazon and adjacent areas of the Atlantic and Pacific Oceans (from 10° N to 10° S) during 2015–2018 using column-averaged atmospheric CO_2 concentration (XCO_2) data from NASA's Orbital Carbon Observatory (OCO-2) (Fig. 3f). The annual growth rates of XCO_2 over the Brazilian Amazon in 2016 (0.87 ppm), 2017 (1.80 ppm) and 2018 (1.79 ppm) were substantially lower than that in 2015 (3.51 ppm) (Fig. 3f and Extended Data Figs. 6 and 9). This suggested that the XCO_2 gradient between the Amazon and surrounding oceans was more negative and was consistent with enhanced CO_2 uptake after the 2015 El Niño.

AGB losses from both deforestation and degradation

The loss of AGB observed in a 0.25° grid cell can be a mix of deforestation, the reduction of biomass density from a suite of other processes, and a contribution from non-forest biomes, the latter having a smaller contribution to grid-cell AGB because of the low AGB of short vegetation. AGB decreases in the Brazilian Amazon have been attributed to direct human-induced deforestation, selective logging[35], forest fragmentation and associated edge effects[36], forest fires[27], and mortality from climatic disturbances such as storms[37] and drought[38,39]. Here we define forest degradation to include all these mechanisms that do not result in deforestation.

The contributions of deforestation and forest degradation to AGB losses cannot be explicitly separated within each 0.25° grid cell, but we performed a simple calculation based on a method reported by Harris et al.[40] (Methods and Fig. 5). Out of the cumulative gross AGB losses (4.45 Pg C) over the study period, we estimated that ~27% (1.18 Pg C) result from deforestation and ~73% (3.27 Pg C) from forest degradation, the latter being composed of 2.88 Pg C in grid cells with deforestation and 0.39 Pg C in the grid cells with no deforestation. Previous studies[9,41] from local inventories and bookkeeping models[40] estimated that forest degradation

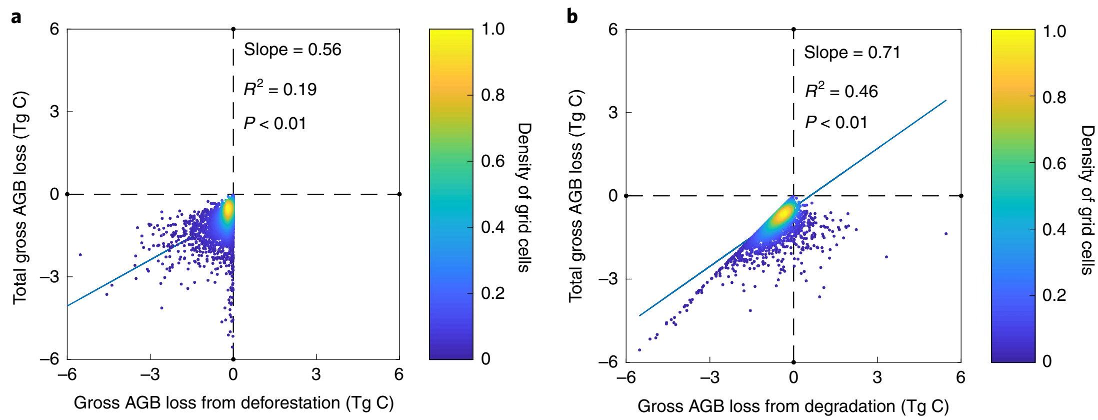

Fig. 5 | Total gross AGB loss from deforestation and forest degradation in those grid cells with forest area loss ($n = 4{,}830$) during 2010–2019 in the Brazilian Amazon. a, Linear relationship between gross AGB loss from deforestation and total gross AGB loss. **b**, Linear relationship between gross AGB loss from degradation and total gross AGB loss. We define forest degradation to include all the mechanisms (such as selective logging, forest fires and mortality from climatic disturbances such as storms and drought) that do not result in full deforestation.

contributed about 29% (ref. [9]) or 18–40% (ref. [41]) to the gross AGB losses in the Brazilian Amazon (Supplementary Table 1), which was less than our top-down estimate of 0.25° L-VOD AGB loss. This can be explained by the full spatial coverage of the entire Brazilian Amazon, and because we included 'degradation' from climatic disturbances. Our result is in agreement with two previous studies[13,42] (Supplementary Table 1). Aragão et al.[42] presented a bottom-up carbon balance for the Brazilian Amazon decomposing each flux and separating the drought effect, which showed that forest degradation contributed 65% to the AGB losses in the 2000s. Baccini et al.[13] used Landsat-based forest cover data during 2003–2014 and estimated that forest degradation contributes 69% to the AGB losses in tropical forests. Long-term forest degradation areas (337,427 km^2) surpassed deforestation (308,311 km^2) in the Brazilian Amazon during 1992–2014 (ref. [32]). According to our estimate, AGB losses from forest degradation are substantial and need to be explicitly included in the global carbon budget assessments[43]. Reducing forest degradation must be a policy priority in the Brazilian Amazon to reach the requirement of Reducing Emissions from Deforestation and Forest Degradation (REDD+) and the carbon emission reduction commitment of the 2015 Paris Agreement.

In areas of intact forests (defined as having a >99% persistent forest cover), AGB losses during 2010–2019 amounted to 0.10 $Mg\,C\,ha^{-1}\,yr^{-1}$ and were found to be substantially associated with fire and water deficit (Extended Data Fig. 10). The AGB density change over intact forests was close to the average (0.06 $Mg\,C\,ha^{-1}\,yr^{-1}$) estimated by the forest plots networks during 2000–2011 (ref. [10]). During 2010–2015, intact forest AGB changes were highly temporally associated with water deficit ($R^2 = 0.81$, $P < 0.01$). During 2015–2019, although the water deficit was reduced, forest AGB continued to decrease due to the legacy effects of drought and a doubling of forest fires compared with 2010–2014, which is supported by field measurements[44–46].

Forest conservation is a challenging task under severe droughts and governmental policies that threaten Amazon forests[47]. Here, we used two new satellite data products to quantify spatial–temporal changes in AGB and forest area in the Brazilian Amazon. The strong spatial–temporal consistency between annual AGB and FAF within individual grid cells during 2010–2019 enables us to determine the relative contributions of deforestation and forest degradation to the losses in AGB[13,48] (potential carbon emissions to the atmosphere) over a long period[44–46]. Large AGB losses in 2015–2016 and large AGB gains in 2011 and 2017 show that the forests are geographically divergent in their sensitivity and resilience to changes in climate, land use and disturbance. Continued land use change[7,26], increased climate extremes in the coming decades[38,39] and new Brazilian governmental policies may reduce the capacity of the forests to sequester carbon[10,11] and make it more challenging to achieve the objectives of the REDD+ programme. To effectively manage, conserve and monitor tropical forests, it is essential to fully integrate in situ, citizen-science, aerial and space-borne data. Recently launched and future space-borne platforms that measure characteristics of vegetation canopy and structure (Global Ecosystem Dynamics Investigation[49]) and atmospheric CO_2 concentration and chlorophyll fluorescence (OCO-2/3 (ref. [30]), TROPOspheric Monitoring Instrument[50] and Geostationary Carbon Cycle Observatory (GeoCarb)[51]) are expected to help us better address these challenges.

Online content

Any methods, additional references, Nature Research reporting summaries, source data, extended data, supplementary information, acknowledgements, peer review information; details of author contributions and competing interests; and statements of data and code availability are available at https://doi.org/10.1038/s41558-021-01026-5.

Received: 6 April 2020; Accepted: 12 March 2021;
Published online: 29 April 2021

References

1. Xiao, X. M., Biradar, C. M., Czarnecki, C., Alabi, T. & Keller, M. A simple algorithm for large-scale mapping of evergreen forests in tropical America, Africa and Asia. *Remote Sens.* **1**, 355–374 (2009).
2. Pan, Y. D. et al. A large and persistent carbon sink in the world's forests. *Science* **333**, 988–993 (2011).
3. Saatchi, S. S. et al. Benchmark map of forest carbon stocks in tropical regions across three continents. *Proc. Natl Acad. Sci. USA* **108**, 9899–9904 (2011).
4. Davidson, E. A. et al. The Amazon basin in transition. *Nature* **481**, 321–328 (2012).
5. Jenkins, C. N., Pimm, S. L. & Joppa, L. N. Global patterns of terrestrial vertebrate diversity and conservation. *Proc. Natl Acad. Sci. USA* **110**, E2602–E2610 (2013).
6. Mitchard, E. T. A. The tropical forest carbon cycle and climate change. *Nature* **559**, 527–534 (2018).
7. Fearnside, P. M. Brazilian politics threaten environmental policies. *Science* **353**, 746–748 (2016).
8. Fearnside, P. M. *Business as Usual: A Resurgence of Deforestation in the Brazilian Amazon* (Yale School of Forestry & Environmental Studies, 2017).
9. Berenguer, E. et al. A large-scale field assessment of carbon stocks in human-modified tropical forests. *Glob. Change Biol.* **20**, 3713–3726 (2014).

10. Brienen, R. J. W. et al. Long-term decline of the Amazon carbon sink. *Nature* **519**, 344–348 (2015).
11. Doughty, C. E. et al. Drought impact on forest carbon dynamics and fluxes in Amazonia. *Nature* **519**, 78–82 (2015).
12. Baccini, A. et al. Estimated carbon dioxide emissions from tropical deforestation improved by carbon-density maps. *Nat. Clim. Change* **2**, 182–185 (2012).
13. Baccini, A. et al. Tropical forests are a net carbon source based on aboveground measurements of gain and loss. *Science* **358**, 230–234 (2017).
14. *PRODES Legal Amazon Deforestation Monitoring System* (INPE, 2018); http://www.obt.inpe.br/OBT/assuntos/programas/amazonia/prodes
15. Hansen, M. C. et al. High-resolution global maps of 21st-century forest cover change. *Science* **342**, 850–853 (2013).
16. Tyukavina, A. et al. Types and rates of forest disturbance in Brazilian Legal Amazon, 2000–2013. *Sci. Adv.* **3**, e1601047 (2017).
17. Qin, Y. et al. Improved estimates of forest cover and loss in the Brazilian Amazon in 2000–2017. *Nat. Sustain.* **2**, 764–772 (2019).
18. Seymour, F. & Harris, N. L. Reducing tropical deforestation. *Science* **365**, 756–757 (2019).
19. Richards, P., Arima, E., VanWey, L., Cohn, A. & Bhattarai, N. Are Brazil's deforesters avoiding detection? *Conserv. Lett.* **10**, 470–476 (2017).
20. Fan, L. et al. Satellite-observed pantropical carbon dynamics. *Nat. Plants* **5**, 944–951 (2019).
21. Brandt, M. et al. Satellite passive microwaves reveal recent climate-induced carbon losses in African drylands. *Nat. Ecol. Evol.* **2**, 827–835 (2018).
22. Wigneron, J.-P. et al. Tropical forests did not recover from the strong 2015–2016 El Niño event. *Sci. Adv.* **6**, eaay4603 (2020).
23. Wigneron, J.-P. et al. SMOS-IC data record of soil moisture and L-VOD: historical development, applications and perspectives. *Remote Sens. Environ.* **254**, 112238 (2021).
24. Qin, Y. W. et al. Annual dynamics of forest areas in South America during 2007–2010 at 50 m spatial resolution. *Remote Sens. Environ.* **201**, 73–87 (2017).
25. Ferrante, L. & Fearnside, P. M. Brazil's new president and 'ruralists' threaten Amazonia's environment, traditional peoples and the global climate. *Environ. Conserv.* **46**, 261–263 (2019).
26. Artaxo, P. Working together for Amazonia. *Science* **363**, 323–323 (2019).
27. Aragão, L. E. O. C. et al. 21st century drought-related fires counteract the decline of Amazon deforestation carbon emissions. *Nat. Commun.* **9**, 536 (2018).
28. Nunes, S., Oliveira, L., Siqueira, J., Morton, D. C. & Souza, C. M. Unmasking secondary vegetation dynamics in the Brazilian Amazon. *Environ. Res. Lett.* **15**, 034057 (2020).
29. Hilker, T. et al. Vegetation dynamics and rainfall sensitivity of the Amazon. *Proc. Natl Acad. Sci. USA* **111**, 16041–16046 (2014).
30. Liu, J. et al. Contrasting carbon cycle responses of the tropical continents to the 2015–2016 El Nino. *Science* **358**, eaam5690 (2017).
31. Giardina, F. et al. Tall Amazonian forests are less sensitive to precipitation variability. *Nat. Geosci.* **11**, 405–409 (2018).
32. Matricardi, E. A. T. et al. Long-term forest degradation surpasses deforestation in the Brazilian Amazon. *Science* **369**, 1378–1382 (2020).
33. Yang, Y. et al. Post-drought decline of the Amazon carbon sink. *Nat. Commun.* **9**, 3172 (2018).
34. Gatti, L. V. et al. Drought sensitivity of Amazonian carbon balance revealed by atmospheric measurements. *Nature* **506**, 76–80 (2014).
35. Asner, G. P. et al. Selective logging in the Brazilian Amazon. *Science* **310**, 480–482 (2005).
36. Silva, C. H. L.Jr et al. Persistent collapse of biomass in Amazonian forest edges following deforestation leads to unaccounted carbon losses. *Sci. Adv.* **6**, eaaz8360 (2020).
37. Espírito-Santo, F. D. B. et al. Size and frequency of natural forest disturbances and the Amazon forest carbon balance. *Nat. Commun.* **5**, 3434 (2014).
38. Lewis, S. L., Brando, P. M., Phillips, O. L., van der Heijden, G. M. F. & Nepstad, D. The 2010 Amazon drought. *Science* **331**, 554–554 (2011).
39. Jiménez-Muñoz, J. C. et al. Record-breaking warming and extreme drought in the Amazon rainforest during the course of El Niño 2015–2016. *Sci. Rep.* **6**, 33130 (2016).
40. Harris, N. L. et al. Baseline map of carbon emissions from deforestation in tropical regions. *Science* **336**, 1573–1576 (2012).
41. Aguiar, A. P. D. et al. Land use change emission scenarios: anticipating a forest transition process in the Brazilian Amazon. *Glob. Change Biol.* **22**, 1821–1840 (2016).
42. Aragão, L. E. O. C. et al. Environmental change and the carbon balance of Amazonian forests. *Biol. Rev.* **89**, 913–931 (2014).
43. Friedlingstein, P. et al. Global carbon budget 2019. *Earth Syst. Sci. Data* **11**, 1783–1838 (2019).
44. Silva, C. V. J. et al. Estimating the multi-decadal carbon deficit of burned Amazonian forests. *Environ. Res. Lett.* **15**, 114023 (2020).
45. Silva, C. V. J. et al. Drought-induced Amazonian wildfires instigate a decadal-scale disruption of forest carbon dynamics. *Phil. Trans. R. Soc. B* **373**, 20180043 (2018).
46. Barlow, J., Peres, C. A., Lagan, B. O. & Haugaasen, T. Large tree mortality and the decline of forest biomass following Amazonian wildfires. *Ecol. Lett.* **6**, 6–8 (2003).
47. Fuchs, R. et al. Why the US–China trade war spells disaster for the Amazon. *Nature* **567**, 451–454 (2019).
48. Hansen, M. C., Potapov, P. & Tyukavina, A. Comment on 'Tropical forests are a net carbon source based on aboveground measurements of gain and loss'. *Science* **363**, eaar3629 (2019).
49. Dubayah, R. et al. The Global Ecosystem Dynamics Investigation: high-resolution laser ranging of the Earth's forests and topography. *Sci. Remote Sens.* **1**, 100002 (2020).
50. Doughty, R. et al. TROPOMI reveals dry-season increase of solar-induced chlorophyll fluorescence in the Amazon forest. *Proc. Natl Acad. Sci. USA* **116**, 22393–22398 (2019).
51. Moore, B. III et al. The potential of the Geostationary Carbon Cycle Observatory (GeoCarb) to provide multi-scale constraints on the carbon cycle in the Americas. *Front. Environ. Sci.* **6**, 109 (2018).
52. *Landsat* (NASA, USGS, 2019); https://landsat.gsfc.nasa.gov/news/media-resources

Publisher's note Springer Nature remains neutral with regard to jurisdictional claims in published maps and institutional affiliations.

Methods

Annual AGB dataset during 2010–2019. In situ measurements of forest AGB dynamics in the Amazon are limited to local forest inventory plots and seasonal direct biometric measurement plots[9–11]. Several studies have combined datasets from both forest inventory plots and remote sensing to generate spatial maps of forest AGB estimates at multiyear time frames[3,12,53], on the basis of canopy height estimates from the Geoscience Laser Altimeter System lidar sampling strips and vegetation indices from optical images (MODIS). The recently developed L-VOD AGB dataset is one of the major satellite-based data sources for monitoring interannual changes in AGB in the tropical regions[20,21,54,55].

The L-VOD AGB data product was derived from the SMOS passive microwave satellite images L-VOD ascending product (version 1.6) developed by the French National Institute for Agricultural Research and the Center for the Study of the Biosphere from Space[21,54,55]. Our previous work by Fan et al.[20] used both ascending observations (acquired at 6:00) and descending observations (acquired at 18:00) over the pan-tropic zone. L-VOD has diurnal dynamics because of leaf water content changes in each day. Here, we used the ascending observations, because at 6:00 the water-refilling process through plant xylem restores the leaf water potential to values close to the root-zone soil water potential, and an equilibrium is reached in the soil–plant–atmosphere continuum[56]. As a result, the ascending observations at 6:00 are less sensitive to plant water stress than the descending observations at 18:00 and are more pertinent to monitoring AGB[20]. The use of only ascending observations was possible in this study, as many subdaily observations were available over the Brazilian Amazon, which is an area that is very little impacted by noisy microwave interferences at the L-band[20]. L-VOD also has seasonal dynamics, as vegetation canopy changes over seasons. Several steps of data filtering were applied to retrieve relatively robust and stable annual estimates (mean and median), and all calculations are detailed in Fan et al.[20].

Here, we used the maximum L-VOD (L-VODmax, defined as the 95% percentile in each year), which occurs mostly in the wet season. During the wet season, the L-VODmax data are relatively independent of annual changes in the dielectric properties of vegetation, which may be assumed to be relatively constant from year to year. Note that we computed L-VOD changes for individual grid cells over years, and it is not our primary task to investigate spatial variations in these dielectric properties. In the long term, these properties may not be constant, as there are changes in vegetation types. But over ten years, we can assume that in a given grid cell, the average vegetation moisture content and dielectric properties during the wet period are about constant. We know that this is not a perfect assumption. However, this assumption was found to be quite well supported by the signatures of the intact forests (FAF > 99% each year), which have stable temporal L-VOD and L-VODmax at the selected sites (Supplementary Fig. 3) and over the whole Brazilian Amazon (Supplementary Fig. 4). There are seasonal changes in L-VOD, but it recovers to the same value each year during the wet period, which suggests that changes in L-VODmax are due only to biomass changes and not to changes in the dielectric properties.

As in Fan et al.[20], the SMOS L-VOD was converted to carbon density using previously published biomass maps[3,12,53] as references via regressions between the annual median of L-VOD (2011) and AGB maps: annual median L-VOD values were converted into the unit of carbon density ($\mathrm{Mg\,C\,ha^{-1}}$) and then averaged. Here, we calculated two sets of L-VOD AGB products for each year using the equations (equation (1) and Supplementary Table 2) generated on the basis of L-VOD in 2011 and two biomass maps generated by Saatchi et al.[3] and Baccini et al.[12] of the tropical Americas, and we then averaged them to get annual AGB maps during 2010–2019. As for the L-VOD product, the L-VOD AGB dataset has a spatial resolution of ~25 km. Fan et al.[20] have done extensive spatial uncertainty analyses of AGB and AGB changes, including internal uncertainties associated with the L-VOD-derived AGB estimates and external uncertainties associated with different reference biomass maps and biomass stocks at continental scales. Combining the internal and external errors, the relative spatial uncertainties associated with AGB and the AGB changes are on the order of 20–30% over the tropics and continents[20].

$$\mathrm{AGB} = a \times \frac{\arctan\left(b \times (\mathrm{VOD} - c)\right) - \arctan(-b \times c)}{\arctan\left(b \times (\mathrm{Inf} - c)\right) - \arctan\left(-b \times c\right)} + d \qquad (1)$$

where a, b, c and d are four best-fit parameters and VOD is the yearly L-VOD data. The yearly L-VOD data calculated for 2011 were used in equation (1), as described by Rodriguez-Fernandez et al.[55], because 2011 was the first complete year after the SMOS commissioning phase.

The remote sensing datasets that we used in our study provide temporally continuous changes in AGB and forest area, but all optical, active and passive microwave images used to estimate AGB encounter various degrees of saturation where forest biomass is very high. However, the L-VOD AGB dataset saturates only at ~200 $\mathrm{Mg\,C\,ha^{-1}}$ (ref. [22]), which, according to Saatchi et al.[3] and Baccini et al.[12], happens only at 2.47% and 0.01%, respectively, of total pixels. Compared with previous studies that used high-frequency VOD (LPRM, LPDR applied to AMSR-E/2)[57,58], the L-VOD AGB dataset (version 2.0) shows a strong relationship between changes in AGB and changes in FAF (Fig. 2).

Annual forest maps during 2010–2019. We generated annual maps of forests in South America during 2007–2010 at 50-m spatial resolution, using the images from the Advanced Land Observing Satellite (ALOS) PALSAR and time series data from the MOD13Q1 Terra Vegetation Indices data product at 16-day temporal resolution and 250-m spatial resolution[24]. We use the Food and Agriculture Organization's forest definition in our forest mapping studies—that is, forest is a land parcel (0.5 ha or larger) with 10% or more tree cover and with tree height >5 metres at their maturity. The resultant annual PALSAR/MODIS forest map in 2010 has high accuracy (>90%) using images with very high spatial resolution and 2-m land cover maps[17,24]. Here, we used the canopy height and canopy cover percentage datasets retrieved from the direct measurements of the three-dimensional canopy structure from the Geoscience Laser Altimeter System observations on board NASA's ICESat-1 (ref. [59]) to assess the 50-m PALSAR/MODIS forest map in the Brazilian Amazon in 2010 in terms of the Food and Agriculture Organization's forest definition. The derived ICESat-1 canopy cover percentage showed almost no bias when compared with airborne lidar estimates and was sensitive to signal dynamics over dense forests, even when canopy cover exceeded 80%. The ICESat-based canopy height and canopy cover percentage estimates were able to better characterize footprint-level canopy conditions than the existing products derived from conventional optical remote sensing[59]. There are 1.1 million ICESat-1 site observations in the Brazilian Amazon. We found that 98.5% of the PALSAR/MODIS forest pixels had canopy height >5 metres and 94.4% of the PALSAR/MODIS forest pixels had canopy cover percentage >10% (Supplementary Fig. 5). Overall, 93.8% of the PALSAR/MODIS forest pixels had canopy height >5 metres and canopy cover percentage >10% (Supplementary Figs. 5 and 6).

We developed a pixel- and phenology-based algorithm to identify and map evergreen forests in individual years[1,17]. The algorithm was based on the canopy phenology from analyses of the time-series enhanced vegetation index (EVI) and Land Surface Water Index (LSWI) from the eight-day 500-m MOD09A1 data product[1,17]. A unique physical feature of evergreen forests is that they have green leaves throughout the year, which is well captured by the time-series EVI and LSWI data in a year. We applied the algorithm to time-series MOD09A1 data over individual pixels in a year and generated annual maps of evergreen forests in the Brazilian Amazon from 2000 to 2019 in the cloud computing platform Google Earth Engine[17]. Limited by the data availability, the forest map for 2019 was generated on the basis of MOD09A1 imagery from 1 January to 3 December 2019. We carried out a temporal consistency check procedure that uses a three-year moving window filter to remove the noise in individual pixels and increase temporal consistency of evergreen forest maps. We further calculated the annual gross loss and gain of forest area on the basis of the forest map in 2001 after excluding all the pixels without cloud-free observations[17].

$$\mathrm{EVI} = 2.5 \times \frac{\rho_{\mathrm{NIR}} - \rho_{\mathrm{red}}}{\rho_{\mathrm{NIR}} + 6 \times \rho_{\mathrm{red}} - 7.5 \times \rho_{\mathrm{blue}} + 1} \qquad (2)$$

$$\mathrm{LSWI} = \frac{\rho_{\mathrm{NIR}} - \rho_{\mathrm{SWIR}}}{\rho_{\mathrm{NIR}} + \rho_{\mathrm{SWIR}}} \qquad (3)$$

where ρ_{blue}, ρ_{red}, ρ_{NIR} and ρ_{SWIR} represent land surface reflectance values from MOD09A1 blue, red, near-infrared and short-wave infrared bands, respectively.

The evergreen forest maps had relatively high overall accuracy (~97%) in the Brazilian Amazon in 2000 and 2010 on the basis of the extensive high-spatial-resolution ground reference maps[17]. The evergreen forest loss and gain also have relatively high accuracy on the basis of 2,000 stratified random sample pixels. The overall accuracy of the evergreen forest loss and gain are 97.79% (±0.64%) and 99.18% (±0.27%), respectively. We aggregated the 50-m PALSAR/MODIS forest map into the 500-m FAF map and compared the areas and spatial consistency between the evergreen forest maps and the PALSAR/MODIS forest maps in the Brazilian Amazon during 2007–2010. The evergreen forests and the PALSAR/MODIS forests reached over 98% consistency in the forest area and forest spatial distribution[17]. Annual maps of evergreen forests in the Brazilian Amazon during 2000–2017 were reported in a recent study[17], and we extended the dataset to 2019 in this study, using the same method. We also compared the 25-m PALSAR-based forest areas developed by the Japan Aerospace Exploration Agency (JAXA) and the 50-m PALSAR/MODIS forest areas with the MOD100 forest areas in the Brazilian Amazon during 2007–2010 and 2015–2017 (2017 is the newest forest data map). The JAXA forest areas and MOD100 forest areas have good consistency (Supplementary Fig. 7). PALSAR/MODIS forest maps and MOD100 forest maps can therefore be used to analyse the forest area changes in the Brazilian Amazon. A comparison among the PALSAR/MODIS forest maps, the PRODES forest map and the GFW forest maps was already reported[17].

GFW forest area dataset during 2010–2019. Tree cover is defined as vegetation higher than 5 metres. The GFW (version 1.7) product[15] includes a tree cover map in 2000, annual tree cover gross loss in 2001–2019 and total tree cover gross gain in binary for 2001–2012 at a spatial resolution of 30 metres. The GFW products were generated from decision tree algorithms through the analysis of time-series Landsat images acquired during the growing season. The GFW products of 2000–2012 were generated on the basis of Landsat 7 thematic mapper plus (ETM+) images. The GFW products of 2011–2019 were generated on the basis of Landsat 5 thematic mapper, Landsat 7 ETM+ and Landsat 8 Operational Land Imager images and updated methodology. Due to variation in the mapping algorithms and the date of content, tree cover and tree cover gross loss and gain cannot be compared accurately against each other. Comparisons between the original 2001–2010 data and the 2011–2019 update should be performed with caution. The GFW product was evaluated with an overall commission error of 13% and an overall omission error of 12%, though the accuracy varies by biome and thus may be higher or lower in any particular location. The data producers are 75% confident that the loss occurred within the stated year and 97% confident that it occurred within a year before or after (https://www.globalforestwatch.org/map?map=eyJjZW50ZXIiOnsibGF0IjoyNywibG5nIjoxMn0sImJlYXJpbmciOjAsInBpdGNoIjowLCJ6b29tIjoyfQ%3D%3D&modalMeta=tree_cover_loss).

PRODES forest area dataset (2010–2019). The PRODES forest product[14] was generated by the Brazilian National Institute for Space Research to identify annual deforestation and forest area in the Brazilian Amazon. One or two Landsat images as cloud-free as possible are used each year per location. The images are then masked to exclude non-forest and previous deforestation, using the previous year's analysis results. Finally, interpreters delineate deforested polygons (in shapefile format) in the intact primary forests of the previous year. In this study, we used the annual deforestation area statistics in the Brazilian Amazon during 2010–2019 as reported by the National Institute for Space Research.

Atmospheric CO_2 concentration dataset during 2015–2018. We obtained daily XCO_2 data from the NASA OCO-2 (ref. [60]). OCO-2 was launched into orbit on 2 July 2014 and flies in a near-polar orbit as part of the Afternoon Train (A-train) constellation of satellites, with a local overpass time of approximately 13:30. It has been recording spectra in the 0.76 μm, 1.61 μm and 2.05 μm spectral regions on a near-continuous basis for five years. The OCO-2 version 9 XCO_2 dataset[61] during 2015–2018 is publicly available. Only observations with quality flag 0 (that is, 'good') were considered in the Amazon, Atlantic Ocean (latitude 10° S–10° N and longitude 60° W–20° W) and Pacific Ocean (latitude 10° S–10° N and longitude 110° W–85° W) at the same latitude (Supplementary Fig. 8), which avoids soundings with errors due to unscreened clouds and aerosols as well as low signal-to-noise ratio[61]. Individual soundings were aggregated to 1° by 1° along the track to account for correlated errors between soundings that are close to one another in space and time, in line with the conclusions of Worden et al.[62].

Active fire and burned area datasets during 2010–2019. The annual active fire and burned area data in the Brazilian Amazon were calculated using the eight-day 1-km MOD14A2 (version 006)[63] and the monthly 500-m MCD64A1 (version 006)[64], respectively. Limited by the data availability, we used MOD14A2 and MCD64A1 acquired between 1 January and 3 December and between January and October 2019. We first selected active fire observations with nominal and high confidence levels and burned area observations with sufficiently valid data in the reflectance time series. We then generated annual active fire and burned area binary maps if active fire and burned area occurred in a year during 2010–2019.

Annual precipitation dataset and evapotranspiration during 2010–2019. We calculated annual precipitation during 2010–2019 using observations from the Tropical Rainfall Measuring Mission (TRMM), a joint mission between NASA and the JAXA. We used the precipitation from the TRMM 34B2 product with a three-hour temporal resolution and a 0.25° × 0.25° (latitude and longitude) spatial resolution[65]. We calculated the annual evapotranspiration as the sum of the eight-day global terrestrial evapotranspiration from the MOD16A2 V105 product at 1-km pixel resolution[66]. Evapotranspiration is the sum of evaporation and plant transpiration from the Earth's surface to the atmosphere. We then calculated the annual water deficit as the difference between annual total precipitation and evapotranspiration for each year.

MCWD and numbers of dry months. The moist tropical canopy transpires about 100 mm per month, according to the ground measurements in different locations and seasons in the Amazon[27]. Forest is in a water deficit when precipitation is less than 100 mm per month. The annual MCWD is the maximum value of the monthly accumulated water deficit per year, which is a useful indicator of meteorologically induced water stress[27]. We calculated the annual MCWD during 2010–2018 using the monthly precipitation of TRMM 3B43 at 0.25° spatial resolution. We also calculated the number of dry months with a water deficit during 2010–2018 in the Brazilian Amazon.

$$\begin{aligned}&\text{If } \mathrm{WD}_{n-1(i,j)} - E_{(i,j)} + P_{n(i,j)} < 0;\\&\text{then } \mathrm{WD}_{n(i,j)} = \mathrm{WD}_{n-1(i,j)} - E_{(i,j)} + P_{n(i,j)}\\&\text{else } \mathrm{WD}_{n(i,j)} = 0\end{aligned} \tag{4}$$

where WD, E and P are water deficit, evapotranspiration and precipitation, respectively. E is equal to 100 mm per month. i and j are the coordinates (column and row) for the grid cells. n is the number of months each year.

PAR dataset during 2010–2019. We calculated the annual mean values in each year during 2010–2019 using the monthly PAR dataset from the National Centers for Environmental Prediction–Department of Energy (NCEP/DOE) Reanalysis-2, which has a spatial resolution of 1.875° × 1.905° (longitude and latitude). We then resampled the annual mean PAR values into ~25-km × 25-km grid cells using the near resampling approach.

Contributions of deforestation and forest degradation to bulk AGB loss. Forest degradation and deforestation are not two independent processes. Deforestation leads to forest degradation by creating edges and increasing the perimeter of forests exposed to sources of fire ignition, and degraded areas are more likely to be deforested. The gross AGB loss in a grid cell is controlled by gross forest area loss, forest degradation and other mechanisms such as non-forest biomass density changes. For grid cells (~25 km × 25 km) with decreased tree cover fraction, if the tree cover fraction is still larger than 10%, we attributed the AGB loss entirely to degradation. If the tree cover fraction is smaller than or equal to 10%, we attributed the AGB loss to deforestation. From these two end members, we attempted a simple estimate of deforestation versus degradation within each grid cell using the method proposed by ref. [40]. First, we calculate the gross bulk AGB loss in each 0.25° grid cell. Second, we multiply the gross forest area loss during 2011–2019 by the AGB density in 2010 to approximately estimate AGB loss from deforestation. Finally, we calculate the difference between gross AGB loss and this deforestation contribution, and we consider this difference to be from degradation.

$$\Delta\mathrm{AGB}_{\text{Gross loss}} = f(\Delta\mathrm{AGB}_{\text{Gross forest area loss}}, \Delta\mathrm{AGB}_{\text{Degradation}}, \text{Others}) \tag{5}$$

$$\text{If } \mathrm{AGB}_{t+1} - \mathrm{AGB}_t < 0, \text{ then } \Delta\mathrm{AGB}_{\text{Gross loss}} = \sum(\mathrm{AGB}_{t+1} - \mathrm{AGB}_t) 2010 \leq t \leq 2019. \tag{6}$$

$$\Delta\mathrm{AGB}_{\text{Gross forest area loss}} \cong \sum(\text{Gross forest area loss}) \times \mathrm{AGB}_{\text{Density}} \tag{7}$$

$$\Delta\mathrm{AGB}_{\text{Degradation}} \cong \Delta\mathrm{AGB}_{\text{Gross loss}} - \Delta\mathrm{AGB}_{\text{Gross forest area loss}} \tag{8}$$

Statistical analysis and spatial–temporal analysis. The 500-m annual forest maps (500-m spatial resolution) were aggregated into ~25-km × 25-km grid cells in ArcGIS (https://desktop.arcgis.com/en/) version 10.1 to match the spatial resolution of the L-VOD AGB dataset. The total forest area (ha) and the FAF (%) were then calculated within each individual grid cell. To analyse the covariations between annual AGB and FAF changes (Extended Data Fig. 4), six category layers were created on the basis of the FAF map in 2010: 0%, >0% and ≤20%, >20% and ≤40%, >40% and ≤60%, >60% and ≤80%, and >80 and ≤100%. Then, the anomaly values (Z-scores) for the total forest area and the total AGB were calculated in each category during 2010–2019.

The linear relationship model analyses (two-tailed) and the relevant slope, R^2 and P values were calculated between annual AGB and FAF within each grid cell in the Brazilian Amazon during 2010–2019 in MATLAB (https://www.mathworks.com/products/matlab.html) version R2017a. The linear regression slope and spatial R^2 values were calculated between annual FAF and AGB during 2010–2019 using the raster and maptools packages in R (https://www.r-project.org/) version 3.4.2.

Reporting Summary. Further information on research design is available in the Nature Research Reporting Summary linked to this article.

Data availability

The annual evergreen forest maps[67] and AGB maps[68] are freely available in GeoTIFF format at Figshare. The GFW product is available at http://earthenginepartners.appspot.com/science-2013-global-forest. The PRODES forest product is available at http://www.obt.inpe.br/OBT/assuntos/programas/amazonia/prodes. The MOD14A2, MOD16A2 and MCD64A1 products are available at https://lpdaac.usgs.gov/data/. The TRMM product is available at https://pmm.nasa.gov/data-access/downloads/trmm. The PAR product is from the NCEP/DOE 2 Reanalysis data provided by the NOAA/OAR/ESRL PSD, Boulder, Colorado, USA, from their website at https://www.esrl.noaa.gov/psd/.

Code availability

The code for the evergreen forest mapping and spatial correlation analysis are freely available at Figshare[69]. The other data processing and analyses were done mainly in ArcMap (https://desktop.arcgis.com/en/arcmap/).

References

53. Avitabile, V. et al. An integrated pan-tropical biomass map using multiple reference datasets. *Glob. Change Biol.* **22**, 1406–1420 (2016).
54. Fernandez-Moran, R. et al. SMOS-IC: an alternative SMOS soil moisture and vegetation optical depth product. *Remote Sens.* **9**, 457 (2017).
55. Rodriguez-Fernandez, N. J. et al. An evaluation of SMOS L-band vegetation optical depth (L-VOD) data sets: high sensitivity of L-VOD to above-ground biomass in Africa. *Biogeosciences* **15**, 4627–4645 (2018).

56. Konings, A. G. & Gentine, P. Global variations in ecosystem-scale isohydricity. *Glob. Change Biol.* **23**, 891–905 (2017).
57. Liu, Y. Y. et al. Recent reversal in loss of global terrestrial biomass. *Nat. Clim. Change* **5**, 470–474 (2015).
58. Moesinger, L. et al. The global long-term microwave Vegetation Optical Depth Climate Archive (VODCA). *Earth Syst. Sci. Data* **12**, 177–196 (2020).
59. Tang, H. et al. Characterizing global forest canopy cover distribution using spaceborne lidar. *Remote Sens. Environ.* **231**, 111262 (2019).
60. Crisp, D. et al. The on-orbit performance of the Orbiting Carbon Observatory-2 (OCO-2) instrument and its radiometrically calibrated products. *Atmos. Meas. Tech.* **10**, 59–81 (2017).
61. Kiel, M. et al. How bias correction goes wrong: measurement of XCO_2 affected by erroneous surface pressure estimates. *Atmos. Meas. Tech.* **12**, 2241–2259 (2019).
62. Worden, J. R. et al. Evaluation and attribution of OCO-2 XCO_2 uncertainties. *Atmos. Meas. Tech.* **10**, 2759–2771 (2017).
63. Giglio, L. & Justice, C. *MOD14A2 MODIS/Terra Thermal Anomalies/Fire 8-Day L3 Global 1 km SIN Grid V006* (NASA EOSDIS Land Processes DAAC, 2015).
64. Giglio, L., Justice, C., Boschetti, L. & Roy, D. *MCD64A1 MODIS/Terra+Aqua Burned Area Monthly L3 Global 500 m SIN Grid V006* (NASA EOSDIS Land Processes DAAC, 2015).
65. Huffman, G. et al. *Integrated Multi-satellitE Retrievals for GPM (IMERG).* Version 4.4 (NASA's Precipitation Processing Center, 2014); ftp://arthurhou.pps.eosdis.nasa.gov/gpmdata/
66. Running, S., Mu, Q. & Zhao, M. *MOD16A2 MODIS/Terra Net Evapotranspiration 8-Day L4 Global 500 m SIN Grid V006* (NASA EOSDIS Land Processes DAAC, 2017).
67. Qin, Y., Xiao, X. & Wigneron, J.-P. Annual evergreen forest maps in the Brazilian Amazon during 2010–2019. *Figshare* https://doi.org/10.6084/m9.figshare.14115518.v1 (2021).
68. Qin, Y., Xiao, X. & Wigneron, J.-P. Annual aboveground biomass maps in the Brazilian Amazon during 2010–2019. *Figshare* https://doi.org/10.6084/m9.figshare.14115566.v1 (2021).
69. Qin, Y., Xiao, X. & Wigneron, J.-P. Code for evergreen forest and aboveground biomass analyses in the Brazilian Amazon. *Figshare* https://doi.org/10.6084/m9.figshare.14115680.v1 (2021).

Acknowledgements

We thank P. Friedlingstein, N. Vuichard, D. Zhu, M. Kautz and B. Poulter for their comments and discussion regarding the early version of this manuscript. Y.Q. and X.X. were supported by the NASA Land Use and Land Cover Change programme (grant no. NNX14AD78G); the Inter-American Institute for Global Change Research (IAI) (grant no. CRN3076), which is supported by the US National Science Foundation (grant no. GEO-1128040); and the NSF EPSCoR project (grant no. IIA-1301789). Y.Q., X.X., S.C., X.W., R.D. and B.M. were supported by NASA's GeoCarb Mission (GeoCarb Contract no. 80LARC17C0001). J.-P.W. was supported by the SMOS project of the TOSCA Programme from CNES, France (Centre National d'Etudes Spatiales). P.C. and S.S. were supported by the RECCAP2 project, which is part of the ESA Climate Change Initiative (contract no. 4000123002/18/I-NB) and the H2020 European Institute of Innovation and Technology (4C; grant no. 821003). S.S. was supported by the Newton Fund through the Met Office Climate Science for Service Partnership Brazil (CSSP Brazil). M.B. was supported by the European Research Council (ERC) under the European Union's Horizon 2020 research and innovation programme (grant agreement no. 947757 TOFDRY) and a DFF Sapere Aude grant (no. 9064–00049B). L.F. was supported by the National Natural Science Foundation of China (grant nos 41801247 and 41830648) and the Natural Science Foundation of Jiangsu Province (grant no. BK20180806). X.L. was supported by the China Scholarship Council (grant no. 201804910838). F.L. was supported by the Strategic Priority Research Program of the Chinese Academy of Sciences (grant no. XDA20010202).

Author contributions

X.X. and Y.Q. designed the overall study plan. Y.Q. and X.X. prepared the annual evergreen forest maps. J.-P.W., M.B., L.F. and X.L. prepared the annual L-VOD AGB dataset. S.C. prepared the OCO-2 XCO_2 dataset. Y.Q., X.X., X.W., R.D., Y.Z. and F.L. carried out the data processing and analysis. X.X., Y.Q., J.-P.W., P.C., M.B., S.S. and L.F. interpreted the results. Y.Q. and X.X. drafted the manuscript, and all authors contributed to the writing and revision of the manuscript.

Competing interests

The authors declare no competing interests.

Additional information

Extended data is available for this paper at https://doi.org/10.1038/s41558-021-01026-5.

Supplementary information The online version contains supplementary material available at https://doi.org/10.1038/s41558-021-01026-5.

Correspondence and requests for materials should be addressed to X.X. or J.-P.W.

Peer review information *Nature Climate Change* thanks Luiz Aragão, Paulo Brando and Fernando Espírito-Santo for their contribution to the peer review of this work.

Reprints and permissions information is available at www.nature.com/reprints.

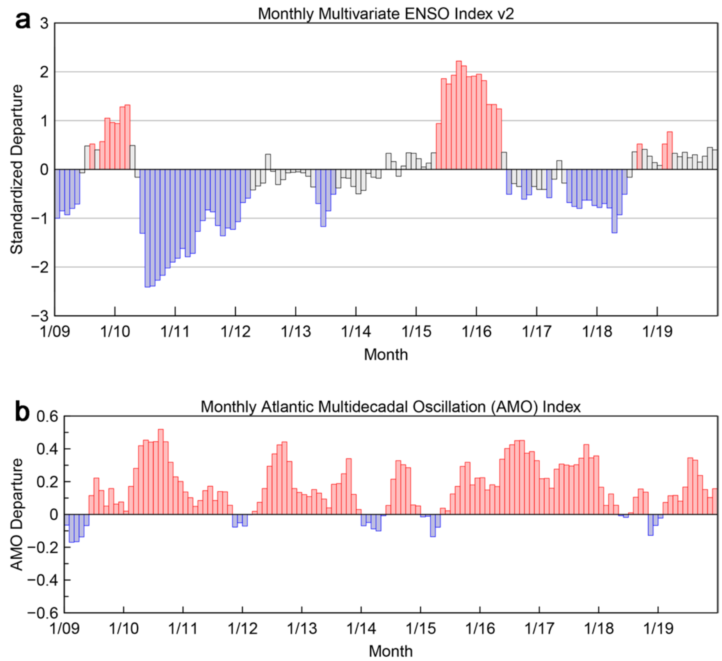

Extended Data Fig. 1 | Monthly multivariate El Niño/Southern Oscillation (ENSO) index and Atlantic Multidecadal Osillation (AMO) index during 2009–2019. a, ENSO index. Warm (red) and cold (blue) periods are based on a threshold of ±0.5. **b**, AMO index. Red and blue colors represent positive and negative data, respectively.

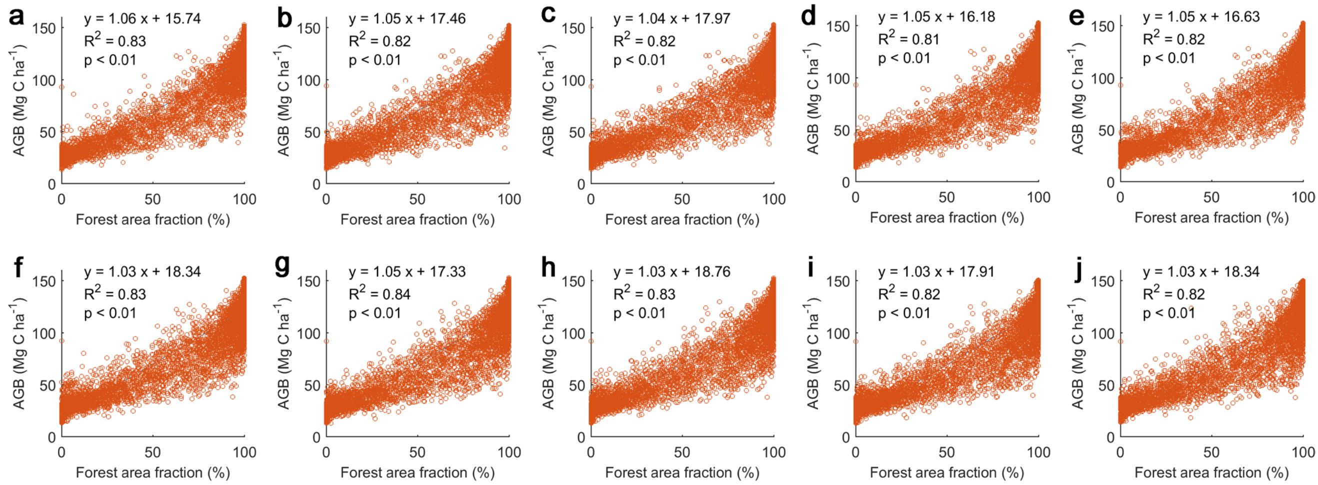

Extended Data Fig. 2 | Two-dimension scatter plots and linear regression relationships between L-VOD AGB and MODIS-based forest area fraction in the Brazilian Amazon during 2010–2019. **a**, 2010. **b**, 2011. **c**, 2012. **d**, 2013. **e**, 2014. **f**, 2015. **g**, 2016. **h**, 2017. **i**, 2018. **j**, 2019 The numbers of grid cells in a year at 0.25° spatial resolution are 5,656.

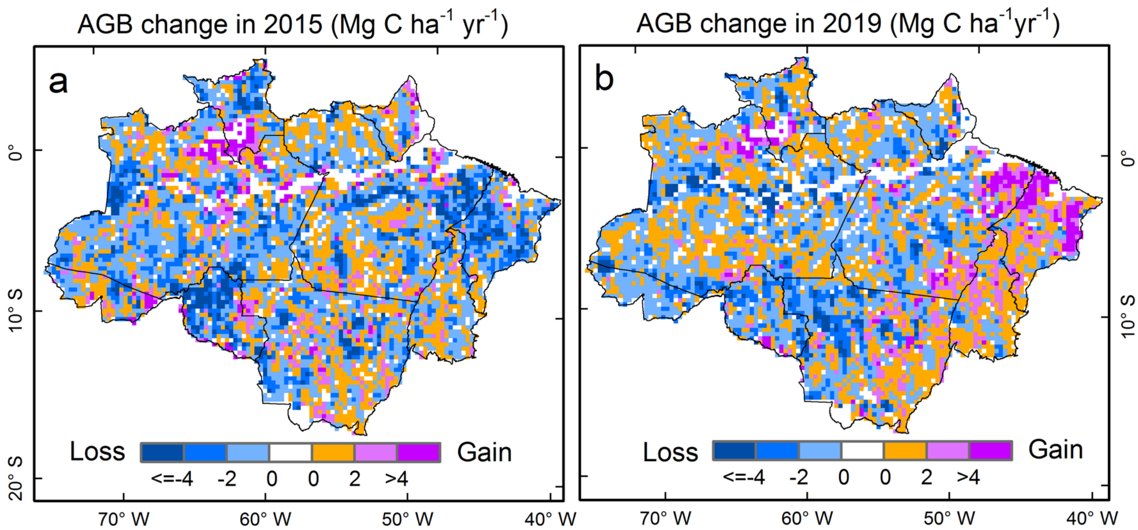

Extended Data Fig. 3 | The spatial distributions of AGB changes in 2015 and 2019. **a**, AGB change in 2015 (Year 2015 - Year 2014). **b**, AGB change in 2019 (Year 2019 - Year 2018).

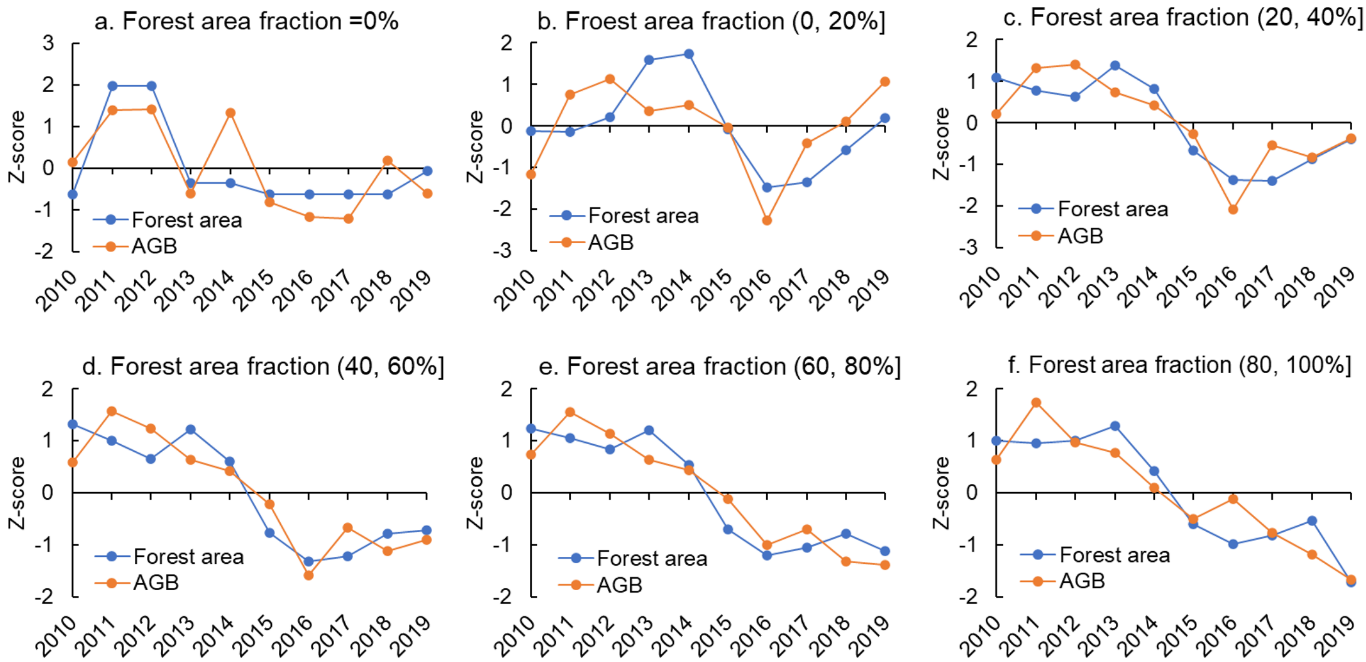

Extended Data Fig. 4 | The relationships between annual average AGB and forest area changes within different initial forest area fraction intervals in 2010. **a**, The region (0.1% of the total area in the Brazilian Amazon) with forest area fraction = 0% ($R^2 = 0.50$, $p < 0.05$, $n = 10$). **b**, The region (15.4%) with forest area fraction (0, 20%] ($R^2 = 0.33$, $p < 0.1$, $n = 10$). **c**, The region (7.3%) with forest area fraction (20, 40%] ($R^2 = 0.67$, $p < 0.01$, $n = 10$). **d**, The region (6.1%) with forest area fraction (40, 60%] ($R^2 = 0.77$, $p < 0.01$, $n = 10$). **e**, The region (8.1%) with forest area fraction (60, 80%] ($R^2 = 0.83$, $p < 0.01$, $n = 10$). **f**, The region (63.0%) with forest area fraction (80, 100%] ($R^2 = 0.78$, $p < 0.01$, $n = 10$).

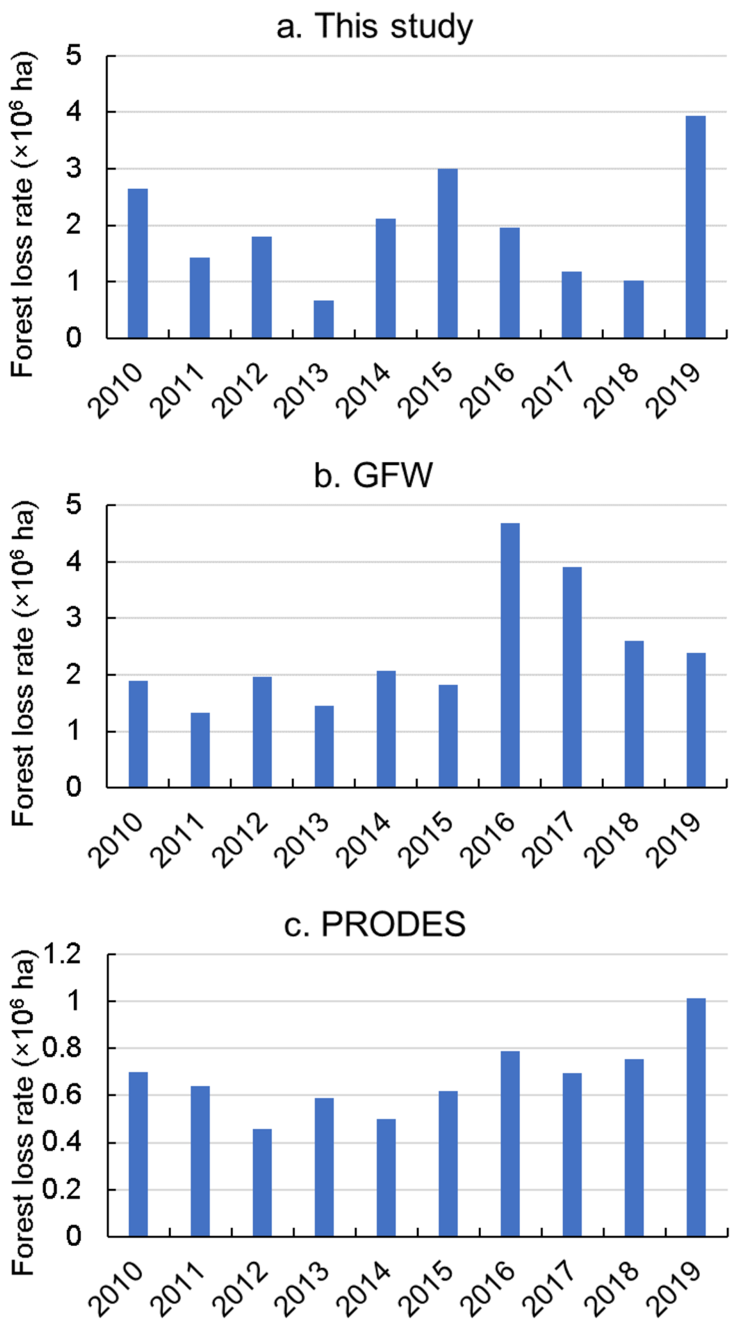

Extended Data Fig. 5 | The annual gross forest area loss estimated by this study, Global Forest Watch (GFW), and PRODES in the Brazilian Amazon during 2010–2019. a, This study. **b**, GFW. **c**, PRODES.

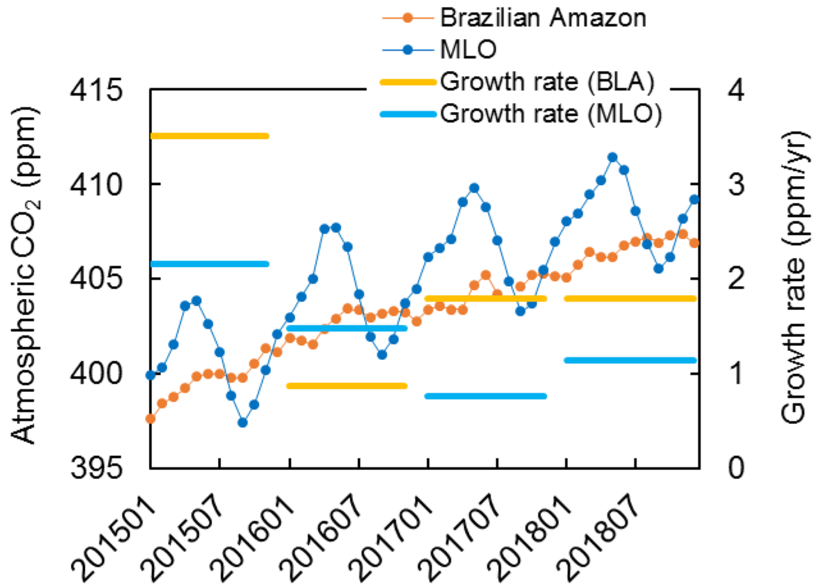

Extended Data Fig. 6 | Interannual variation of atmospheric CO_2 concentration. Time series atmospheric CO_2 concentration and growth rates in the Brazilian Amazon (BLA) and Mauna Loa Observatory (MLO).

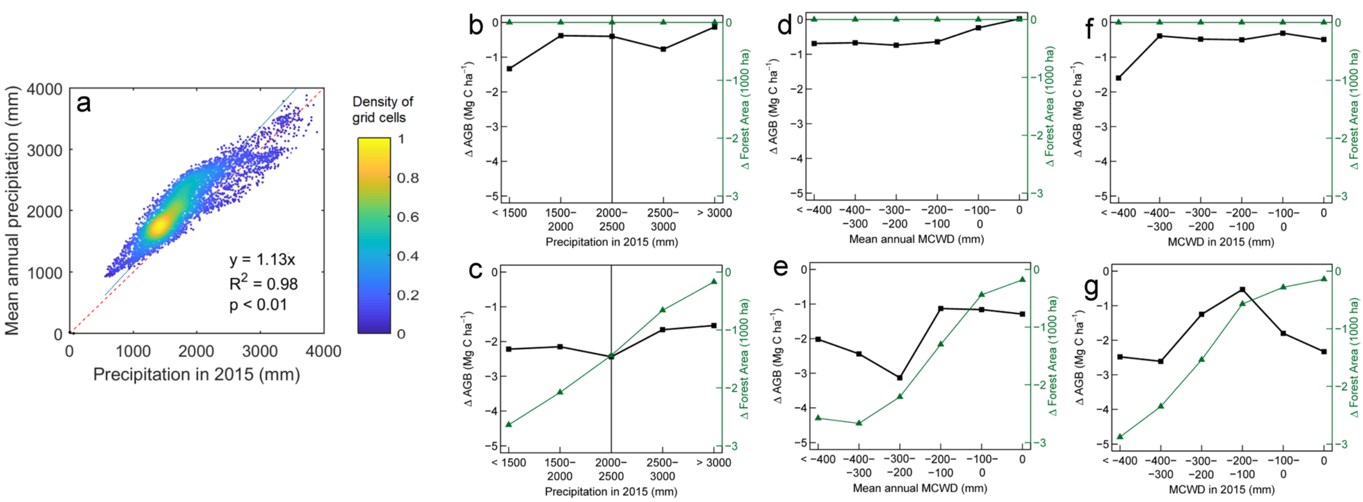

Extended Data Fig. 7 | AGB changes over the two periods of 2010–2013 and 2015–2018 along the precipitation and maximum cumulated water deficit (MCWD) in the Brazilian Amazon. a, Linear regression analysis between precipitation in 2015 and mean annual precipitation during 2010–2019 (n = 5,656). **b**-**c**, Changes of AGB and forest area in those grid cells with zero forest change (**b**) and in those grid cells with [−10, 0)×10^3 ha forest area loss (**c**) over different precipitation intervals in 2015. **d**-**e**, Changes of AGB and forest area in those grid cells with zero forest change (**d**) and in those grid cells with [−10, 0)×10^3 ha forest area loss (**e**) over different mean annual MCWD intervals. **f**-**g**, Changes of AGB and forest area in those grid cells with zero forest change (**f**) and in those grid cells with [−10, 0)×10^3 ha forest area loss (**g**) over different MCWD intervals in 2015.

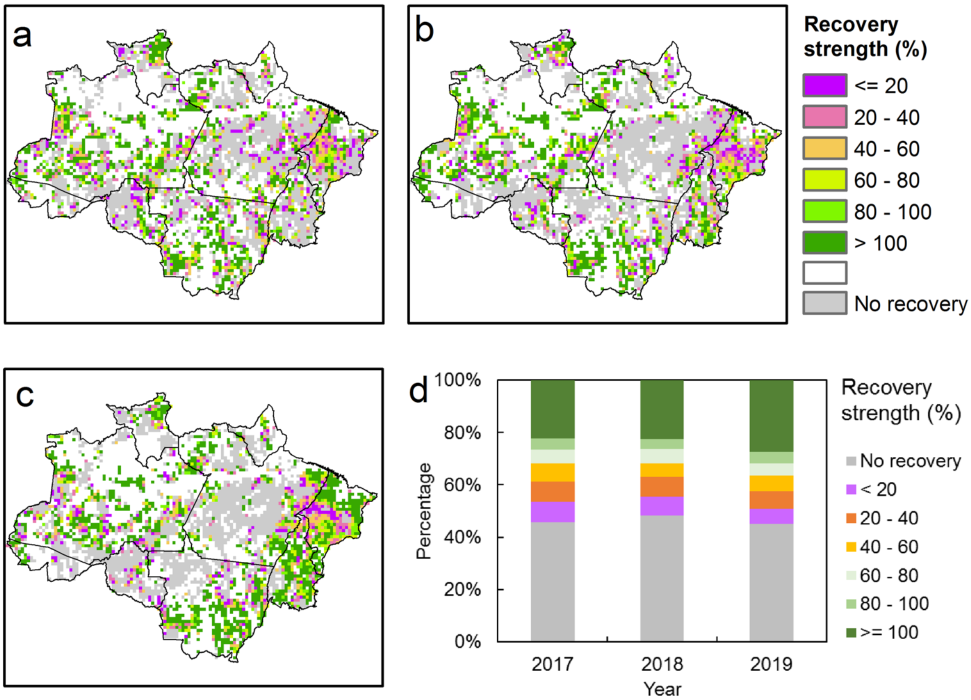

Extended Data Fig. 8 | AGB recovery strength in 2017, 2018, and 2019 after 2015/2016 El Nino. We calculated AGB loss (AGB_{ENSO}) between AGB in 2014 and average AGB in 2015/2016 and AGB gain (AGB_R) between AGB in 2017, 2018, 2019 and average AGB in 2015/2016. The ratio between AGB_R and AGB_{ENSO} is AGB recovery strength. **a**, Recovery strength in 2017. **b**, Recovery strength in 2018. **c**, Recovery strength in 2019. **d**, Area statistics of recovery strength in 2017, 2018, and 2019.

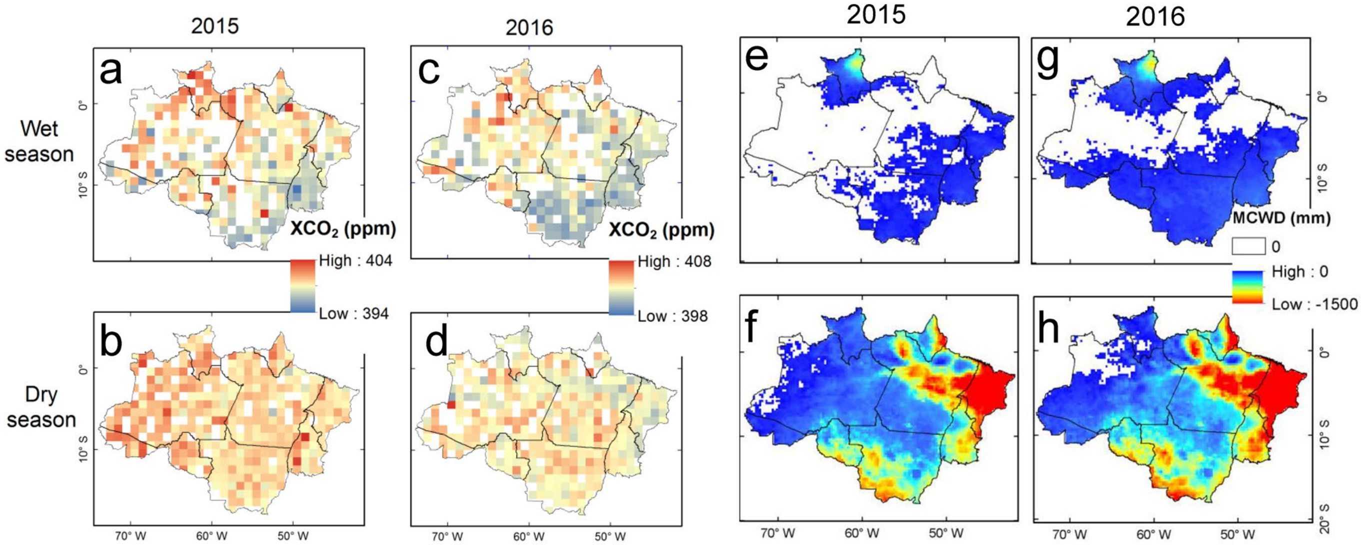

Extended Data Fig. 9 | The spatial distribution maps of the average OCO-2 XCO2 in the wet season and dry season at the spatial resolution of 1° in the Brazilian Amazon in 2015 and 2016. **a**, and (**b**) are the XCO_2 in the wet and dry season in 2015. **c**, and (**d**) are the XCO_2 in the wet and dry season in 2016. **e**, and (**f**) are the MCWD in the wet season and dry season in 2015. **g**, and (**h**) are the MCWD in the wet and dry season in 2016. The wet season covers the period from January to May. The dry season cover the period from July to November.

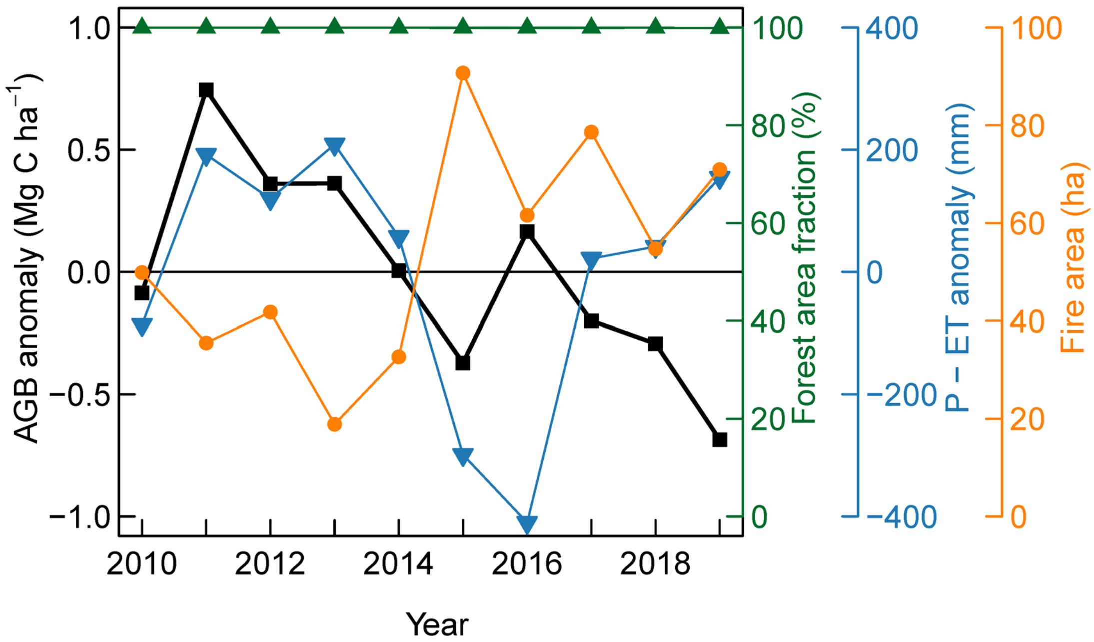

Extended Data Fig. 10 | AGB anomaly, forest area fraction, (Precipitation (P) – Evapotranspiration (ET)) anomaly, and fire area in the intact forests in the Brazilian Amazon during 2010–2019. The anomalies of AGB and (P-ET) are calculated using the references of the average AGB and average (P-ET) values during 2010–2019.

nature research

Corresponding author(s): Xiangming Xiao, Jean-Pierre Wigneron

Last updated by author(s): Feb 26, 2021

Reporting Summary

Nature Research wishes to improve the reproducibility of the work that we publish. This form provides structure for consistency and transparency in reporting. For further information on Nature Research policies, see Authors & Referees and the Editorial Policy Checklist.

Statistics

For all statistical analyses, confirm that the following items are present in the figure legend, table legend, main text, or Methods section.

n/a	Confirmed	
☒	☐	The exact sample size (n) for each experimental group/condition, given as a discrete number and unit of measurement
☐	☒	A statement on whether measurements were taken from distinct samples or whether the same sample was measured repeatedly
☐	☒	The statistical test(s) used AND whether they are one- or two-sided *Only common tests should be described solely by name; describe more complex techniques in the Methods section.*
☒	☐	A description of all covariates tested
☒	☐	A description of any assumptions or corrections, such as tests of normality and adjustment for multiple comparisons
☐	☒	A full description of the statistical parameters including central tendency (e.g. means) or other basic estimates (e.g. regression coefficient) AND variation (e.g. standard deviation) or associated estimates of uncertainty (e.g. confidence intervals)
☐	☒	For null hypothesis testing, the test statistic (e.g. F, t, r) with confidence intervals, effect sizes, degrees of freedom and P value noted *Give P values as exact values whenever suitable.*
☒	☐	For Bayesian analysis, information on the choice of priors and Markov chain Monte Carlo settings
☒	☐	For hierarchical and complex designs, identification of the appropriate level for tests and full reporting of outcomes
☐	☒	Estimates of effect sizes (e.g. Cohen's d, Pearson's r), indicating how they were calculated

Our web collection on statistics for biologists contains articles on many of the points above.

Software and code

Policy information about availability of computer code

Data collection	The annual aboveground biomass and forest maps are generated based on the freely available satellite images, including the L-band Soil Moisture and Ocean Salinity (https://directory.eoportal.org/web/eoportal/satellite-missions/content/-/article/smos) and the MOD09A1 (https://lpdaac.usgs.gov/products/mod09a1v006/)
Data analysis	We use ArcGIS 10.1 (https://www.arcgis.com/index.html), R (https://www.r-project.org/), ENVI/IDL 5.2 (https://www.harrisgeospatial.com/), and Matlab R2017a (https://www.mathworks.com/products/matlab.html) to carry out data analysis.

For manuscripts utilizing custom algorithms or software that are central to the research but not yet described in published literature, software must be made available to editors/reviewers. We strongly encourage code deposition in a community repository (e.g. GitHub). See the Nature Research guidelines for submitting code & software for further information.

Data

Policy information about availability of data

All manuscripts must include a data availability statement. This statement should provide the following information, where applicable:

- Accession codes, unique identifiers, or web links for publicly available datasets
- A list of figures that have associated raw data
- A description of any restrictions on data availability

The annual evergreen forest maps (https://figshare.com/s/802f977f8c73994da238) and AGB maps (https://figshare.com/s/49bb5f9bdf3f241965d5) are freely available in the GeoTIFF format at Figshare. The GFW product is available at http://earthenginepartners.appspot.com/science-2013-global-forest. The PRODES forest product is available at http://www.obt.inpe.br/OBT/assuntos/programas/amazonia/prodes. MOD14A2, MOD16A2, and MCD64A1 products are available at https://lpdaac.usgs.gov/data/. The TRMM product is available at https://pmm.nasa.gov/data-access/downloads/trmm. The PAR product is from the NCEP/DOE 2 Reanalysis data provided by the NOAA/OAR/ESRL PSD, Boulder, Colorado, USA, from their Web site at https://www.esrl.noaa.gov/psd/.

Field-specific reporting

Please select the one below that is the best fit for your research. If you are not sure, read the appropriate sections before making your selection.

☐ Life sciences ☐ Behavioural & social sciences ☒ Ecological, evolutionary & environmental sciences

For a reference copy of the document with all sections, see nature.com/documents/nr-reporting-summary-flat.pdf

Ecological, evolutionary & environmental sciences study design

All studies must disclose on these points even when the disclosure is negative.

Study description	Spatial-temporal dynamics of aboveground biomass (AGB) and forest area affect the carbon cycle, climate, and biodiversity in the Brazilian Amazon. Here we investigate inter-annual changes of AGB and forest area by analyzing satellite-based annual AGB and forest area datasets. We found the gross forest area loss was larger in 2019 than in 2015, possibly due to recent loosening of forest protection policies. However, net AGB loss was three times smaller in 2019 than in 2015. During 2010-2019, the Brazilian Amazon had a cumulative gross loss of 4.45 Pg C against a gross gain of 3.78 Pg C, resulting in net AGB loss of 0.67 Pg C. Forest degradation (73%) contributed three times more to the gross AGB loss than deforestation (27%), given that the areal extent of degradation exceeds deforestation. This indicates that forest degradation has become the largest process driving carbon loss and should become a higher policy priority.
Research sample	Our study did not use sample.
Sampling strategy	Our study did not use sample.
Data collection	*Describe the data collection procedure, including who recorded the data and how.*
Timing and spatial scale	Our study used (1) annual aboveground biomass maps at 0.25 degree during 2010-2019, and (2) annual evergreen forest maps at 500 m spatial resolution during 2010-2019 and were then aggregated into 0.25 degree.
Data exclusions	No data was excluded from analysis.
Reproducibility	Our study is not based on experiments. We analyzed annual aboveground biomass maps and forest maps derived from satellite images in the Brazilian Amazon.
Randomization	Our study is not based on experiments, so no randomization was needed.
Blinding	Our study is not based on experiments, so no blinding was needed.

Did the study involve field work? ☐ Yes ☒ No

Reporting for specific materials, systems and methods

We require information from authors about some types of materials, experimental systems and methods used in many studies. Here, indicate whether each material, system or method listed is relevant to your study. If you are not sure if a list item applies to your research, read the appropriate section before selecting a response.

Materials & experimental systems

n/a	Involved in the study
☒	☐ Antibodies
☒	☐ Eukaryotic cell lines
☒	☐ Palaeontology
☒	☐ Animals and other organisms
☒	☐ Human research participants
☒	☐ Clinical data

Methods

n/a	Involved in the study
☒	☐ ChIP-seq
☒	☐ Flow cytometry
☒	☐ MRI-based neuroimaging